THE JOURNAL OF
Obstetrics and Gynaecology Research

doi:10.1111/jog.12324 J. Obstet. Gynaecol. Res. Vol. 40, No. 5: 1197–1204, May 2014

Mutational analysis of *FOXL2* p.C134W and expression of bone morphogenetic protein 2 in Japanese patients with granulosa cell tumor of ovary

Kumiko Oseto[1], Nobuhiro Suzumori[1], Ryutaro Nishikawa[1], Hiroshi Nishikawa[1], Atsushi Arakawa[1], Yasuhiko Ozaki[1], Hidekazu Asai[2], Michiyasu Kawai[3], Kimio Mizuno[4], Satoru Takahashi[5], Tomoyuki Shirai[6], Chisato Yamada-Namikawa[7], Makoto Nakanishi[7], Hiroaki Kajiyama[8], Fumitaka Kikkawa[8] and Mayumi Sugiura-Ogasawara[1]

[1]*Department of Obstetrics and Gynecology,* [5]*Experimental Pathology and Tumor Biology,* [7]*Department of Cell Biology, Nagoya City University Graduate School of Medical Sciences,* [4]*Red Cross Nagoya Daiichi Hospital,* [6]*Nagoya City Rehabilitation Center,* [8]*Department of Obstetrics and Gynecology, Nagoya University Graduate School of Medicine, Nagoya,* [2]*Tosei Municipal Hospital, Seto and* [3]*Toyohashi Municipal Hospital, Toyohashi, Japan*

Abstract

Aim: To assess whether *FOXL2* p.C134W mutation may play a role in the development of human ovarian tumors in the Japanese, we investigated the *FOXL2* codon 134 mutation and protein expression of inhibin-α, bone morphogenetic protein 2 (BMP2) and follistatin (FST) in Japanese patients with granulosa cell tumor (GCT) of the ovary and other ovarian tumors.

Methods: We analyzed 114 tumor tissues from ovarian tumors, including 44 adult-type and two juvenile-type GCT of the ovary and 68 ovarian tumors by DNA sequencing. Immunohistochemistry was also performed in the adult and juvenile GCT tissues by immunostaining inhibin-α, BMP2 and FST.

Results: We found the *FOXL2* p.C134W mutation in 27 out of 44 (61.4%) adult-type GCT of the ovary, but none in other ovarian tumors. Histologically, all of the adult-type GCT sections were positive for inhibin-α, and the expression of BMP2 and FST was detected in 14 of 44 (31.8%) and zero of 47 (0%), respectively. No significant differences regarding the diagnosed age, preoperative serum carbohydrate antigen 125 levels, or BMP2 immunopositivity between the *FOXL2* p.C134W mutation-positive and mutation-negative were found in the adult-type GCT patients.

Conclusion: Our findings suggest that *FOXL2* p.C134W mutation-positive adult-type GCT of the ovary may not be common in the Japanese as compared to the previous data.

Key words: bone morphogenetic protein 2, follistatin, granulosa cell tumor, inhibin, ovarian tumor.

Introduction

FOXL2 encodes a forkhead transcription factor which is selectively expressed in the mesenchyme of developing mouse eyelids and in the adult ovarian follicles.[1] FOXL2 is one of the earliest markers of ovarian differentiation, and its expression persists into adulthood. FOXL2 is required for the normal development of

Received: June 27 2013.
Accepted: October 11 2013.
Reprint request to: Dr Nobuhiro Suzumori, Department of Obstetrics and Gynecology, Nagoya City University Graduate School of Medical Sciences, 1 Kawasumi, Mizuho-ku, Mizuho-cho, Nagoya 467-8601, Japan. Email: og.n.suz@med.nagoya-cu.ac.jp
Conflict of interest: None declared.

granulosa cells.[2] All mutations that have been described in *FOXL2* are germ line loss-of-function mutations and are associated with blepharophimosis, ptosis and epicanthus inversus syndrome with premature ovarian failure, in particular granulosa cell failure.[1,3,4]

Granulosa cell tumor (GCT) of the ovary is a sex cord-stromal tumor and it accounts for less than 5% of all ovarian cancers.[5] The GCT are usually low-grade malignancies, but the patients have a high risk of recurrences occurring up to 40 years after primary tumor resection.[6] They are distinct from other ovarian carcinomas in hormonal activity and they have the ability to secrete estrogen, inhibin and Müllerian inhibiting substance. Because molecular pathogenesis of GCT remains unclear, significant clinical prognostic markers have not been discovered. For the patients with advanced stage or recurrent GCT, the efficacy of chemotherapy has been limited, so more effective therapeutic approaches are needed.[7]

Recent studies have revealed that a somatic *FOXL2* codon 134 mutation (c.402C>G, p.C134W) is a feature shared by 94–97% of adult GCT, which suggests that it is constitutes an early event in their pathogenesis.[8–12] Lima *et al.* reported that *FOXL2* p.C134W mutation was identified in 40% of male, adult GCT.[13] Recent findings suggest that the genes differentially expressed in GCT are significantly enriched for known *FOXL2* target genes, consistent with the prevalence of *FOXL2* p.C134W somatic mutation in these tumors.[14]

In the present study, we investigate whether adult and juvenile GCT have similar incidences of *FOXL2* p.C134W in the Japanese population compared with the previous studies abroad. Recent data suggest a model in which FOXL2 and bone morphogenetic protein 2 (BMP2) cooperate to ensure correct expression of the follistatin (*FST*) gene in the developing ovary.[15] FST is a specific binding protein of activin and is involved in the regulation of pathophysiological functions, including early embryonic development and differentiation of ovarian granulosa cells.[16,17] A recent study suggested that FST protein expression was immunohistochemically detected in 53% of ovarian cancers, and that high serum levels of FST were found in the patients.[18] Therefore, we study histopathological features of the *FOXL2* p.C134W mutation-positive and -negative GCT regarding the expression of BMP2 and FST immunohistochemically. We herein report the *FOXL2* p.C134W mutation and expression of inhibin-α, BMP2 and FST in Japanese patients with GCT of the ovary.

Methods

The study was performed between 2009 and 2012 in around Nagoya, Japan. Enrolled subjects were women with GCT of the ovary (GCT, $n = 46$; 44 adult-type GCT and two juvenile-type GCT), surface epithelial–stromal ovarian cancer ($n = 63$), germ cell tumor ($n = 3$) and others ($n = 2$). The postoperative paraffin-embedded 114 samples were reviewed in this study. The study protocol was approved by the institutional review board of Nagoya City University. Benign ovarian tumor patients with no evidence of malignancies, endometriosis or pelvic adhesions were excluded from the study. In all of the tissues, the diagnosis of human ovarian tumors was confirmed histologically.

Patient charts were reviewed to obtain data regarding age, diagnosis, histology, grade, International Federation of Gynecologists and Obstetricians (FIGO) stage, pathological tumor–node–metastasis stage and prognosis. All of the patients were surgically staged according to the FIGO staging system. The pathology for all the patients with cancer was reviewed by a gynecological pathologist. In most GCT cases, preoperative serum were collected and measured for carbohydrate antigen 125 (CA125) levels.

Until now, all of the somatic *FOXL2* mutations in tumors have been detected at nucleotide sequences c.402C>G in exon 1, which would result in amino acid substitutions at 134 (p.C134W). We analyzed part of exon 1 of the *FOXL2* gene by direct sequencing using the genomic DNA. Genomic DNA from all patients was obtained from routinely processed formalin-fixed and paraffin-embedded (FFPE) biopsy specimens. DNA was extracted from the specimens by digestion with lysis buffer including proteinase K in order to lyse all materials. It was vortexed and continuously shaken at short intervals during overnight incubation at 56°C. The DNA quality and quantity was measured by Nanodrop (Thermo Scientific, Waltham, MA, USA) and a total of 200 ng was used for sequencing. The sense and antisense polymerase chain reaction (PCR) and sequence primers for *FOXL2* were 5′-CCGCCACA ACCTCAGCCTC-3′ and 5′-CGCCGGTAGTTGCCCT TCTC-3′, respectively, with a product size of 156 bp. The exon 1 of the human *FOXL2* gene were amplified by PCR and sequenced using the Big Dye Terminator v3.1 Cycle Sequencing kit (ABI Prism, Applied Biosystems, Foster City, CA, USA) on a 3100 automated sequencer. Seventeen out of the 44 adult GCT samples failed to be sequenced, so those PCR DNA fragments were cloned using the pTA2 Vector (Target Clone

-Plus-, TOYOBO, Japan) and the inserts were sequenced, from the 5′- and 3′-ends, using the automated DNA sequencer. At least four clones were sequenced and analyzed in each GCT sample.

With use of ovarian tissue sections from 44 adult GCT and two juvenile GCT, immunohistochemistry for inhibin-α, BMP2 and FST was performed. We analyzed inhibin-α, BMP2 and FST using the anti-inhibin-α monoclonal antibody (dilution 1:50; Abcam, Cambridge, MA, USA), anti-BMP2 polyclonal antibody (1:100; Bioworld Technology, Minneapolis, MN, USA) and anti-FST monoclonal antibody (1:50; R&D Systems, Minneapolis, MN, USA). The immunohistochemistry procedures have been described in our previous studies.[19] The sections were counterstained with hematoxylin–eosin, mounted, and photographed using an Olympus BX51 microscope and DP70 camera (Olympus, Tokyo, Japan).

The statistical analysis was carried out using SPSS version 19.0 software, and $P < 0.05$ was considered to denote statistical significance.

Results

We found that the *FOXL2* p.C134W mutation was present in 27 out of the 44 (61.4%) adult-type tumors, but in none of the two juvenile-type GCT (Table 1, Fig. 1). In adult-type GCT using FFPE samples, sequencing of 17 out of the 44 samples, so subsequently the PCR DNA fragments were subcloned with the use of the pTA2 Vector and the inserts were sequenced, from the 5′- and 3′-ends by DNA sequencer. The other ovarian samples were successfully sequenced by DNA direct sequencing.

In the other ovarian tumors, except for adult-type GCT, for the mutational analysis based on histology (surface epithelial–stromal ovarian cancer [$n = 63$], germ cell tumor [$n = 3$], juvenile GCT [$n = 2$] and others [$n = 2$]), we performed the mutational analysis by direct sequencing (Table 1). However, none of the samples from the non-GCT or juvenile-type GCT patients showed any evidence of the mutations by direct sequencing, which indicates that the *FOXL2* c.402C>G, pC134W mutation is a somatic one, but that has been confirmed with germ line studies.

In directly sequenced 29 GCT samples including two juvenile GCT, the 17 samples were *FOXL2* p.C134W mutation-positive. Of the 17 adult GCT samples that were subcloned and sequenced, 10 were *FOXL2* mutation-positive. All of the 17 *FOXL2* mutation-negative and the 27 mutation-positive adult-type GCT were histologically considered to be consistent with GCT, and we confirmed that they were immunohistochemically inhibin-α-positive (Fig. 2). Table 2 shows characteristics of the adult-type GCT patients regarding the diagnosed age, *FOXL2* pC134W mutation, BMP2 immunostaining, preoperative serum CA125 levels, FIGO stage and prognosis. The adult-type GCT group ($n = 44$; 52.4 ± 15.7 years, mean age ± standard deviation) and the non-GCT group ($n = 68$, 53.7 ± 12.9 years) were matched for age ($P = 0.562$). No significant differences of diagnosed age between the *FOXL2* p.C134W mutation-positive ($n = 27$, 53.3 ± 15.2 years) and the mutation-negative ($n = 17$, 51.1 ± 16.8 years) cases were found ($P = 0.828$) in the adult-type GCT patients. In 17 of 39 (43.9%) adult-type GCT patients, preoperative serum CA125 levels were elevated using the cut-off of 30 U/mL. In addition, no

Table 1 *FOXL2* p.C134W mutations in human ovarian tumors

Organ	Type of tumor		*n*	*FOXL2* codon 134	
				Mutation	Mutation (%)
Ovary	GCT, adult type		44	27	61.4
	GCT, juvenile type		2	0	0
	Surface epithelial–stromal tumor	Serous adenocarcinoma	18	0	0
		Mucinous adenocarcinoma	9	0	0
		Endometrioid adenocarcinoma	7	0	0
		Clear cell adenocarcinoma	6	0	0
		Serous tumor of borderline malignancy	2	0	0
		Mucinous tumor of borderline malignancy	15	0	0
		Clear cell tumor of borderline malignancy	1	0	0
		Others	5	0	0
	Germ cell tumor		3	0	0
	Others		2	0	0
Total			114	27	23.7

GCT, granulosa cell tumor.

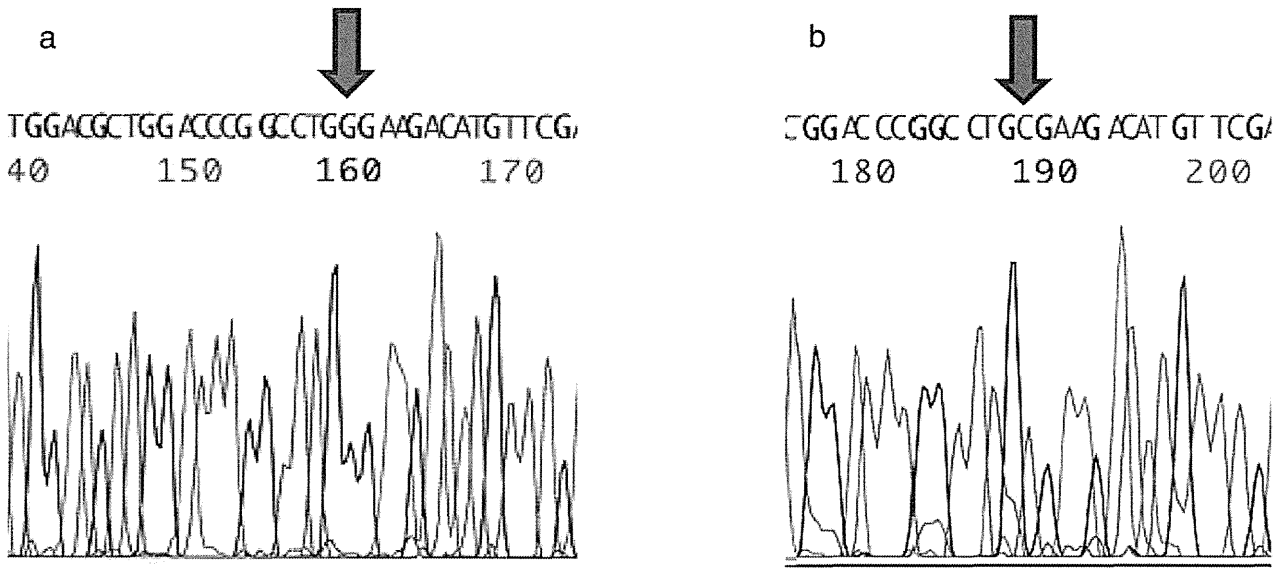

Figure 1 Mutations of *FOXL2* gene codon 134 (p.C134W) in granulosa cell tumors (GCT). Direct DNA sequencing analyses of adult-type GCT with the (a) *FOXL2* mutation and (b) without *FOXL2* mutation.

significant differences of preoperative serum CA125 levels between the *FOXL2* p.C134W mutation-positive ($n = 24$, 86.8 ± 116 U/mL) and the mutation-negative ($n = 15$, 56.4 ± 109 U/mL) cases were identified with the Mann–Whitney non-parametric *U*-test ($P = 0.356$).

With immunohistochemistry, we examined the expression status of inhibin-α, BMP2 and FST using the adult GCT tissue sections. All of the adult and juvenile GCT sections were positive for inhibin-α (Fig. 2c,d). In the adult-type GCT, 14 of 44 (31.8%) and zero of 44 (0%) GCT were positive for BMP2 and FST, respectively (Fig. 2e,f, Table 2). No expression of FST was found in the two juvenile GCT either, although the human pituitary specimen provided as a positive control was positive. After performing Fisher's exact test, there was no significant difference in BMP2 immunopositivity between the adult-type GCT with and without the *FOXL2* p.C134W mutation (Table 3, $P > 0.05$).

Discussion

Granulosa cell tumors of the ovary are thought to arise from normal proliferating granulosa cells of the late preovulatory follicle and they exhibit many morphological and biochemical features of these cells.[20] GCT are distinct from other ovarian carcinomas in the hormonal activity in the ability to secrete estrogen and inhibin. All of our adult-type GCT samples were immunohistochemically inhibin-α-positive, but our findings suggest that the frequency of *FOXL2* p.C134W mutation-positive adult-type GCT of ovary may not be common in the Japanese.

Although the *FOXL2* p.C134W mutation has been recently reported a feature shared by 94–97% of adult GCT,[8–12] D'Angelo *et al.* found the mutation in 70% of the adult GCT in non-Japanese.[21] They also suggests that the *FOXL2* p.C134W mutation and mRNA expression are of prognostic importance in both adult and juvenile GCT.[21] Our present data of the *FOXL2* mutation may be common enough in the Japanese. In contrast, we speculate that the lower proportions identified in these studies may be related to using FFPE specimens and the possibility of tumor heterogeneity being evident when doing so. Recent insights into the molecular pathogenesis of GCT may open a way for new efforts in the development of more targeted therapeutic strategies for GCT patients.[14]

The high frequency with which the *FOXL2* p.C134W mutation occurs in adult-type GCT, along with its absence from juvenile-type GCT and other human malignancies, is suggestive of an oncogenic or gain-of-function mutation and that the mutation is pathognomonic for adult GCT.[20] In our cases, the adult-type GCT sample that was 14 years old was *FOXL2* mutation-positive, although two juvenile-type GCT were mutation-negative.

Shah *et al.* suggested the possibility that negative expression of inhibin may be a feature of *FOXL2*

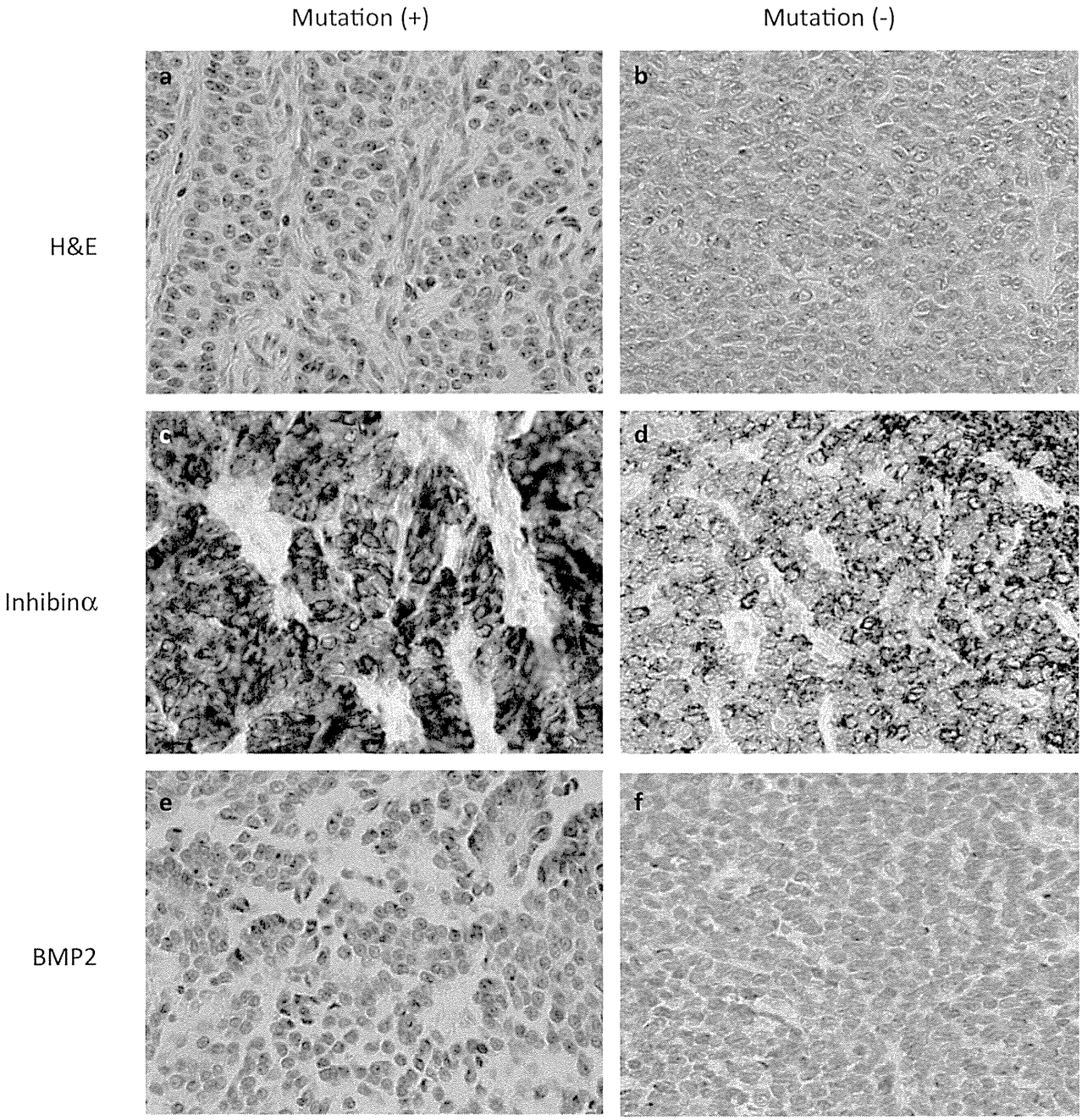

Figure 2 Histopathology and immunohistochemistry of adult-type granulosa cell tumors (GCT). (a,b) The adult-type GCT samples with (a) positive and (b) negative *FOXL2* p.C134W mutation (hematoxylin–eosin). The GCT were histologically considered to be consistent with GCT. (c,d) Immunohistochemistry for inhibin-α. Both of the GCT samples (c) positive and (d) negative for the *FOXL2* p.C134W mutation expressed inhibin-α in the cytosol. (e,f) In the case of bone morphogenetic protein 2 (BMP2), the adult-type GCT samples showed cytoplasmic immunopositivity. The BMP2 immunostained GCT samples are the *FOXL2* p.C134W mutation (e) positive and (f) negative (original magnification, ×400).

Table 2 Characteristics of 44 adult-type granulosa cell tumor patients

Diagnosed age	*FOXL2* mutation	BMP2	CA125 (U/mL)	FIGO stage	pTNM	Survival/death
64	+	+	27.2	Ic	pT1cNxM0	Survival
57	+	+	113.0	Ia	pT1aNxMo	Survival
57	+	+	79.0	Ia	pT1aNXM0	Survival
56	+	+	419.0	Ic	pT1cNXM0	Survival
56	+	+	26.0	Ia	pT1aNXM0	Survival
35	+	+	7.2	Ia	pT1ANxM0	Survival
43	+	+	7.0	IIIa	pT3ANxMo	Survival
73	+	+	4.0	Ia	pT1aN0M0	Survival
14	+	+	28.0	Ic	pT1cNxM0	Survival
59	+	+	4.2	Ia	pT1aNxMo	Survival
56	+	−	20.0	Ia	pT1aNXMO	Survival
65	+	−	49.0	Ic	pTIcN0M0	Survival
36	+	−	−	Ic	pT1cNXM0	Survival
62	+	−	−	Ia	pT1aNXM0	Death (DOD)
51	+	−	388.0	IIc	pT2cNxM0	Survival
44	+	−	58.0	IIIa	pT3aNxM0	Survival
70	+	−	74.6	Ia	pT1aNxM0	Survival
28	+	−	17.0	Ic	pT1cNxM0	Survival
80	+	−	17.5	IIc	pT2cNxM0	Survival
75	+	−	141.1	Ia	pT1aNxM0	Survival
43	+	−	8.5	IIc	pT2cNxM0	Survival
36	+	−	10.4	Ia	pT1aNxM0	Survival
64	+	−	166.0	Ia	pT1ANxM0	Survival
61	+	−	190.0	Ic	pTIcN0M0	Survival
60	+	−	210.0	Ic	pT1cN0M0	Death (DOD)
47	+	−	17.9	Ia	pTIaN0M0	Survival
47	+	−	−	Ia	pTIaN0M0	Survival
40	−	+	11.0	Ia	pT1aNxMo	Survival
75	−	+	−	Ia	pTIaN0Mo	Death (Lung cancer)
66	−	+	8.2	Ia	pT1ANxM0	Survival
43	−	+	7.0	Ia	pT1aNXM0	Survival
20	−	−	87.0	Ic	pT1cNxM0	Survival
50	−	−	12.4	Ia	pT1ANxM0	Survival
54	−	−	−	Ia	pT1ANXM0	Survival
47	−	−	60.0	Ia	pT1aNxM0	Survival
45	−	−	13.0	Ia	pT1aN0M0	Survival
62	−	−	55.4	Ic	pT1cNxM0	Survival
19	−	−	441.0	Ia	pT1aNXMO	Survival
72	−	−	35.0	Ic	pT1cNXMX	Survival
61	−	−	23.0	Ia	pT1ANxM0	Survival
29	−	−	8.5	Ia	pT1ANxMo	Survival
62	−	−	54.7	Ia	pT1ANxM0	Survival
60	−	−	16.0	Ia	pT1aNxMo	Survival
63	−	−	14.4	Ia	pT1aNxMo	Survival

BMP2, bone morphogenetic protein 2; CA125, carbohydrate antigen 125; DOD, died of disease; FIGO, International Federation of Gynecology and Obstetrics; pTNM, pathological tumor–node–metastasis.

mutation-negative adult GCT, although Kim *et al.* did not find any difference in inhibin-α expression according to the *FOXL2* mutation in the GCT.[8,9] Our findings suggest that inhibin-α expression did not differentiate *FOXL2* p.C134W mutation status, because our data showed that all of the adult-type and juvenile-type GCT were inhibin-α-positive, immunohistochemically.

The clinically accepted serum marker for ovarian cancer, the most common cause of death among gynecologic malignancies, is CA125, which in the majority of cases is found to be elevated.[22,23] In 43.9% of our adult-type GCT patients, preoperative serum CA125 levels were elevated using the cut-off of 30 U/mL. As for the *FOXL2* p.C134W mutation, in the adult-type

Table 3 Relation between *FOXL2* p.C134W mutation and BMP2 immunostaining

		BMP2 immunopositivity +	BMP2 immunopositivity −	Total	*P*
FOXL2	+	10	17	27	NS
Mutation	−	4	13	17	
Total		14	30	44	

BMP2, bone morphogenetic protein 2; NS, not significant.

GCT patients no significant differences of the serum CA125 levels between the *FOXL2* mutation-positive and the mutation-negative cases were identified.

Follistatin was originally identified as an inhibitor of follicle-stimulating hormone secretion[24] and may have an important role in folliculogenesis, ovarian function and differentiation of granulosa cells.[18,25,26] The candidate for the upregulation of *Fst* expression is FOXL2. *FOXL2* encodes a forkhead transcription factor which is selectively expressed in the mesenchyme of developing mouse eyelids and in adult ovarian follicles.[1] Kashimada *et al.* suggest a model in which FOXL2 and BMP2 cooperate to ensure correct expression of *FST* in the developing ovary.[15] In contrast, no FST protein expression of adult-type or juvenile-type GCT was confirmed in this study, although Ren *et al.* reported that FST immunoreactivity was detectable in serous cystadenocarcinoma and endometrioid carcinoma tissue in patients with high serum FST levels.[18]

Ma *et al.* reported that the mRNA and protein expression levels of BMP2 in ovarian cancer tissue were remarkably lower than those in benign ovarian tumors and normal ovarian tissue.[27] In our study, 31.8% of the adult-type GCT were immunohistochemically positive for BMP2, and no significant difference in BMP2 immunopositivity was found between the adult-type GCT with and without the *FOXL2* p.C134W mutation. Recent findings suggested that BMP2 treatment *in vitro* mimicked the effects of carcinoma-associated mesenchymal stem cells (MSC) on cancer stem cells, while inhibiting BMP signaling *in vitro* and *in vivo* partly abrogated MSC-promoted tumor growth.[28] The data also suggests that MSC in the ovarian tumor microenvironment have an expression profile that promotes tumorigenesis and that BMP inhibition may be an effective therapeutic approach for ovarian cancer.

In summary, we found the *FOXL2* p.C134W mutation in 61.4% adult-type GCT of the ovary in Japanese subjects. The expression of BMP2 in the adult-type GCT was immunohistochemically detected in 31.8%, but none of the FST expression was detectable. No significant differences of BMP2 immunopositivity between the *FOXL2* p.C134W mutation-positive and the mutation-negative were found in the patients. Our data suggest that *FOXL2* p.C134W mutation-positive adult-type GCT of the ovary may not be common in the Japanese. Further studies with larger numbers and a wider region of the cases in Japan are now needed to clarify the prevalence of the *FOXL2* p.C134W mutation, the molecular pathogenesis and therapeutic strategies for GCT.

Acknowledgments

The authors would like to thank Kazuhiro Higuchi M.D. and Tadashi Sumi M.D. for their advice and help with collecting samples. This work was supported in part by the Program for Developing the Supporting System for Upgrading Education and Research from the Ministry of Education, Culture, Sports, and Technology of Japan (to N. S.).

References

1. Crisponi L, Deiana M, Loi A *et al.* The putative forkhead transcription factor FOXL2 is mutatedin blepharophimosis/ptosis/epicanthus inversus syndrome. *Nat Genet* 2001; **27**: 159–166.
2. Schmidt D, Ovitt CE, Anlag K *et al.* The murine winged-helix transcription factor Foxl2 is required for granulosa cell differentiation and ovary maintenance. *Development* 2004; **131**: 933–942.
3. De Baere E, Dixon MJ, Small KW *et al.* Spectrum of FOXL2 gene mutations in blepharophimosis-ptosis-epicanthus in versus (BPES) families demonstrates a genotype-phenotype correlation. *Hum Mol Genet* 2001; **10**: 1591–1600.
4. Beysen D, Vandesompele J, Messiaen L, De Paepe A, De Baere E. The human FOXL2 mutation database. *Hum Mutat* 2004; **24**: 189–193.
5. Schumer ST, Cannistra SA. Granulosa cell tumor of the ovary. *J Clin Oncol* 2003; **21**: 1180–1189.
6. East N, Alobaid A, Goffin F, Ouallouche K, Gauthier P. Granulosa cell tumour: A recurrence 40 years after initial diagnosis. *J Obstet Gynaecol Can* 2005; **27**: 363–364.
7. Colombo N, Parma G, Zanagnolo V, Insinga A. Management of ovarian stromal cell tumors. *J Clin Oncol* 2007; **25**: 2944–2951.
8. Shah SP, Kobel M, Senz J *et al.* Mutation of FOXL2 in granulosa-cell tumors of the ovary. *N Engl J Med* 2009; **360**: 2719–2729.
9. Kim MS, Hur SY, Yoo NJ, Lee SH. Mutational analysis of FOXL2 codon 134 in granulose cell tumour of ovary and other human cancers. *J Pathol* 2010; **221**: 147–152.
10. Schrader KA, Gorbatcheva B, Senz J *et al.* The specificity of the FOXL2 c.402C>G somatic mutation: A survey of solid tumors. *PLoS ONE* 2009; **4**: e7988.

11. Benayoun BA, Caburet S, Dipietromaria A *et al.* Functional exporation of the adult ovarian granulosa cell tumor-associated somatic FOXL2 mutation p.Cys134Trp (c.402C>G). *PLoS ONE* 2010; **5**: e8789.
12. Rosario R, Araki H, Print CG, Shelling AN. The transcriptional targets of mutant FOXL2 in granulosa cell tumours. *PLoS ONE* 2012; **7**: e46270.
13. Lima JF, Jin L, de Araujo ARC *et al.* FOXL2 mutations in granulosa cell tumors occurring in males. *Arch Pathol Lab Med* 2012; **136**: 825–828.
14. Benayoun BA, Anttonen M, Lhote D *et al.* Adult ovarian granulosa cell tumor transcriptomics: Prevalence of FOXL2 target genes misregulation gives insights into the pathogenic mechanism of the p.Cys134Trp somatic mutation. *Oncogene* 2013; **32**: 2739–2746.
15. Kashimada K, Pelosi E, Chen H, Schlessinger D, Wilhelm D, Koopman P. FOXL2 and BMP2 act cooperatively to regulate *Follistatin* gene expression during ovarian development. *Endocrinology* 2011; **152**: 272–280.
16. Maguer-Satta V, Bartholin L, Jeanpierre S *et al.* Regulation of human erythropoiesis by activin A, BMP2, and BMP4, members of the TGFβ family. *Exp Cell Res* 2003; **282**: 110–120.
17. Nakamura T, Hasegawa Y, Sugino K *et al.* Follistatin inhibits activin-induced differentiation of rat follicular granulosa cells *in vitro*. *Biochim Biophys Acta* 1992; **1135**: 103–109.
18. Ren P, Chen F-F, Liu H-Y *et al.* High serum levels of follistatin in patients with ovarian cancer. *J Int Med Res* 2012; **40**: 877–886.
19. Suzumori N, Sato M, Yoneda T, Ozaki Y, Takagi H, Suzumori K. Expression of secretory leukocyte protease inhibitor in women with endometriosis. *Fertil Steril* 1999; **72**: 857–867.
20. Jamieson S, Fuller PJ. Molecular pathogenesis of granulosa cell tumors of the ovary. *Endocr Rev* 2012; **33**: 109–144.
21. D'Angelo E, Mozos A, Nakayama D *et al.* Prognostic significance of FOXL2 mutation and mRNA expression in adult and juvenile granulosa cell tumors of the ovary. *Mod Pathol* 2011; **24**: 1360–1367.
22. Jacobs I, Bast RC. The CA-125 tumour associated antigen: A review of the literature. *Hum Reprod* 1989; **4**: 1–12.
23. Berek JS, Bast RC Jr. Ovarian cancer screening. The use of serial complementary tumor markers to improve sensitivity and specificity for early detection. *Cancer* 1995; **76**: 2092–2096.
24. Ueno N, Ling N, Ying SY, Esch F, Shimasaki S, Guillemin R. Isolation and partial characterization of follistatin: A single-chain Mr 35,000 monomeric protein that inhibits the release of follicle-stimulating hormone. *Proc Natl Acad Sci USA* 1987; **84**: 8282–8286.
25. Jorgez CJ, Klysik M, Jamin SP, Behringer RR, Matzuk MM. Granulosa cell-specific inactivation of follistatin causes female fertility defects. *Mol Endocrinol* 2004; **18**: 953–967.
26. Mattukrishna S, Tannetta D, Groome N, Sargent I. Activin and follistatin in female reproduction. *Mol Cell Endocrinol* 2004; **225**: 45–56.
27. Ma Y, Ma L, Guo Q, Zhang S. Expression of bone morphogenetic protein-2 and its receptors in epithelial ovarian cancer and their influence on the prognosis of ovarian cancer patients. *J Exp Clin Cancer Res* 2010; **29**: 85.
28. McLean K, Gong Y, Choi Y *et al.* Human ovarian carcinoma–associated mesenchymal stem cells regulate cancer stem cells and tumorigenesis via altered BMP production. *J Clin Invest* 2011; **121**: 3206–3219.

THE JOURNAL OF BIOLOGICAL CHEMISTRY VOL. 289, NO. 17, pp. 11656–11666, April 25, 2014

Mammal-specific H2A Variant, H2ABbd, Is Involved in Apoptotic Induction via Activation of NF-κB Signaling Pathway*[S]

Received for publication, December 10, 2013, and in revised form, February 6, 2014 Published, JBC Papers in Press, February 28, 2014, DOI 10.1074/jbc.M113.541664

Takahiro Goshima[‡1], Midori Shimada[‡1,2], Jafar Sharif[§], Hiromi Matsuo[‡], Toshinori Misaki[‡], Yoshikazu Johmura[‡], Kazuhiro Murata[‡], Haruhiko Koseki[§], and Makoto Nakanishi[‡3]

From the [‡]Department of Cell Biology, Graduate School of Medical Sciences, Nagoya City University, 1 Kawasumi, Mizuho-cho, Mizuho-ku, Nagoya 467-8601, Japan and [§]Development Genetics Group, RIKEN Center for Integrative Medical Sciences (IMS), 1-7-22 Suehiuro-cho, Tsurumi, Yokohama, Kanagawa 230-0045, Japan

Background: H2ABbd is an H2A variant possessing a highly divergent structure. However, the *in vivo* function of H2ABbd is not understood.
Results: Expression of H2ABbd caused DNA damage, induced apoptotis, and finally led to cell death.
Conclusion: H2ABbd caused apoptosis in caspase 3- and NF-κB-dependent manners.
Significance: This work describes a novel role for human H2ABbd in gene regulation and cell death.

Histone variants play specific roles in maintenance and regulation of chromatin structures. H2ABbd, an H2A variant, possesses a highly divergent structure compared with canonical H2A and is highly expressed in postmeiotic germ cells, but its functions in the regulation of gene expression are largely unknown. In the present study, we investigated the cellular phenotype associated with enforced H2ABbd expression. Among H2A variants, H2ABbd specifically caused growth defect in human cells and induced apoptosis. H2ABbd expression resulted in degradation of inhibitor of κB-α and translocation of NF-κB into nuclei, indicating the activation of NF-κB. Intriguingly, NF-κB activity was essential for H2ABbd-induced apoptosis. H2ABbd overexpression resulted in DNA damage after release from G_1/S, progressed through the S phase slowly, and induced apoptosis. Furthermore, gene expression microarray analysis revealed that expression of H2ABbd activates groups of genes involved in apoptosis and postmeiotic germ cell development, suggesting that H2ABbd might influence transcription. Taken together, our data suggest that H2ABbd may contribute to specific chromatin structures and promote NF-κB activation, which could in turn induce apoptosis in mammalian cells.

Genetic information must be stably transmitted during cell divisions through DNA replication followed by rapid packaging of newly synthesized DNA into chromatin. Nucleosomes, the building blocks of chromatin, consist of two pairs of histones, H3-H4 and H2A-H2B, forming an octamer around which DNA is wound (1). Defects in assembly and structure of chromatin may lead to loss of epigenetic information and gross chromosomal rearrangements. However, in order to switch on/off gene expression upon exogenous and endogenous stimuli, remodeling of the chromatin fiber is required to allow/prevent access of transcriptional and epigenetic machineries. One way to achieve this goal is to shuffle canonical histone molecules with histone variants. Previous studies have shown that exchange of canonical histones contributes to a multitude of downstream effects, including alteration in local chromatin organization, chromosome segregation, DNA repair, and transcriptional regulation. This suggests that histone variants might have an important role in chromatin structure and function in general (2).

Histone H2A has several variants with specialized functions. Among them, H2ABbd (H2A Barr body-deficient) is a highly divergent H2A variant (which shares about 48% sequence identity with the canonical H2A) and is found only in mammals (3). Based on its unique structure (3), H2ABbd has been proposed to link specific chromatin states to transcriptional activation (4). Consistent with this notion, recent works showed that H2ABbd was excluded from the inactive X chromosome and colocalized with regions having high levels of acetylated H4 (3). This is further supported by the fact that H2ABbd destabilizes the nucleosome core particles, causing a more relaxed nucleosome core particle conformation (5–8). Indeed, mouse H2ABbd homologue H2AL1 and H2AL2 expressed in postmeiotic cells (9) and H2A.Lap1 are localized at the transcription start sites of active genes (10). Ectopically expressed human H2ABbd in HeLa cells was deposited at intron-exon boundaries, and H2ABbd knockdown cells showed splicing defects, indicating another potential role of this H2A variant in transcriptional regulation through splicing (11).

DNA damage, a potential risk for normal transmission of genetic/epigenetic information, is frequently caused by the collapse of replication forks during DNA replication. To counter such events, mammalian cells are equipped with an elaborate DNA damage response (DDR)[4] mechanism, which functions through precise detection of damaged DNA, rapid transmission of signals to downstream effector molecules to facilitate

* This work was supported by grants from the NEXT program (LS105) and the Naito Foundation (to M. S.).
[S] This article contains supplemental Tables 1–3 and Figs. 1–7.
[1] Both authors contributed equally to this work.
[2] To whom correspondence may be addressed. Tel.: 81-52-853-8146; Fax: 81-52-842-3955; E-mail: midorism@med.nagoya-cu.ac.jp.
[3] To whom correspondence may be addressed. Tel.: 81-52-853-8146; Fax: 81-52-842-3955; E-mail: mkt-naka@med.nagoya-cu.ac.jp.

[4] The abbreviations used are: DDR, DNA damage response; GO, gene ontology; MEF, mouse embryo fibroblast; EGFP, enhanced green fluorescent protein; Dox, doxycycline; ASA, aminosalicylic acid; MNase, micrococcal nuclease.

DNA repair, and in extreme cases cell cycle arrest and apoptosis (12). Importantly, it has been reported that incomplete or aberrant DDR leads to diseases such as malignant transformation by causing genetic mutations and genomic instability. Protein kinases ATM (ataxia-telangiectasia, mutated) and ATR (ATM and Rad3-related) are major players in DDR that function through activation of a plethora of downstream targets, including RPA2, H2AX, 53BP1, Chk1, Chk2, and p53. Among these, the p53 and NF-κB transcription factors play key roles in regulation of cell death and cell survival in response to DNA damage, respectively (13). ATM phosphorylates and stabilizes p53, which is the master regulator of apoptosis. In addition, ATM activates NF-κB by cooperating with its essential modulator, NEMO (14). Intriguingly, although it is widely perceived that NF-κB functions as an antiapoptotic molecule, recent studies indicate that NF-κB may also facilitate apoptosis under certain circumstances.

TSEG-1, a rodent version of H2ABbd, has previously been implicated in induction of cell death in cultured spermatocytes (GC-2spd cells) (15). To investigate this possibility further, we expressed H2ABbd in human cells and found that ectopic expression of H2ABbd led to caspase-dependent apoptosis. Intriguingly, treatment with a NF-κB inhibitor blocked H2ABbd-induced apoptosis, suggesting that NF-κB might play a proapoptotic role in H2ABbd-overexpressing cells. To gain insights into the molecular mechanisms linking H2ABbd overexpression with NF-κB-mediated cell death, we performed gene expression microarray analysis and found that indeed ectopic expression of H2ABbd resulted in up-regulation of a set of apoptosis-related genes. Furthermore, gene ontology (GO) tests revealed that genes involved in development/differentiation as well as factors specific to postmeiotic germ cells (*i.e.* elongating and round spermatids) were preferentially enriched in H2ABbd-expressing cells. Based on these results, we hypothesized that ectopic expression of H2ABbd in somatic cells might cause destabilization of genome integrity, which could potentially lead to activation of the DDR pathway by sensing DNA damage and finally cause cell death by an NF-κB-mediated pathway.

EXPERIMENTAL PROCEDURES

Cell Culture—HeLa cells and MEFs were cultured in DMEM supplemented with 10% FBS RPE cells were cultured in DMEM/F-12 supplemented with 10% FBS. All cells were cultured at 37 °C under 5% CO_2.

Construction of Expression Vectors—EGFP-tagged H2A, H2AX, and H2ABbd expression vectors were constructed. We amplified and subcloned human *H2ABbd* (*H2AFB3*) (GenBank™ accession number NM_080720), *H2A* (*HIST1H2AM*) (GenBank™ accession number NM_003514), and *H2AX* (*H2AFX*) (GenBank™ accession number NM_002105) as follows.

EGFP fragments were cut from pEGFP-C1 using NheI and EcoRI restriction endonucleases. Blunt ends were created after NheI single digestion, before EcoRI digestion. pENTR1A-EGFP vector was generated by subcloning the EGFP fragment into pENTR1A (Invitrogen) vector that was already digested with KpnI, blunt-ended, and further cleaved with EcoRI.

pENTR1A-EGFP-H2A and -H2AX vectors were constructed by subcloning human *H2A* and *H2AX* genes into pENTR1A-EGFP using EcoRI and EcoRV sites. Human *H2A* and *H2AX* were obtained by PCR amplification from total human cDNA library using primers that introduced EcoRI and EcoRV sites on both flanks of the amplified segment.

EGFP-H2ABbd expression vectors were generated in the following way. First pcDNA3.1-H2ABbd-MBD-NLS poly(A) was generated by cutting EGFP from the pcDNA3.1-EGFP-MBD-NLS poly(A) vector (a gift from Dr. Yuki Okada) using HindIII and NotI restriction endonucleases and by subcloning *H2ABbd* into pcDNA3.1-MBD-NLS poly(A). Human *H2ABbd* genes (having no introns) were obtained by PCR amplification of human genomic DNA using primers that introduce HindIII and NotI sites at the flanking regions. EGFP fragments with HindIII sites at both ends were religated into pcDNA3.1-H2ABbd-MBD-NLS poly(A), resulting in a pcDNA3.1-EGFP-H2ABbd-MBD-NLS poly(A) vector. Finally, EGFP-H2ABbd fragments were cut from pcDNA3.1-EGFP-H2ABbd-MBD-NLS poly(A), using EcoRI and NotI, and ligated into pENTR1A vector digested with the same enzymes, resulting in a pENTR1A-EGFP-H2ABbd vector. pENTR1A-H2A, H2AX, and H2ABbd vectors were incubated with CSIV-TRE-RfA-UbC-KT vectors and LR Clonase enzyme mix (Invitrogen) for 2 h at 25 °C, which produced CSIV-TRE-RfA-UbC-KT EGFP-H2A, H2AX, and H2ABbd.

Construction of FLAG-HA-tagged histone H2ABbd was as follows. *H2ABbd* with XhoI and NotI sites was obtained by PCR amplification of pENTR1A-EGFP-H2ABbd. pOZ-FH-N-H2ABbd was generated by subcloning *H2ABbd* into pOZ-FH-N vector digested with XhoI and NotI.

Next, FLAG-HA-H2ABbd fragments with EcoRI and NotI sites were obtained by PCR amplification of pOZ-FH-N-H2ABbd, digested, and subcloned into pENTR1A that was already cleaved with EcoRI and NotI, producing the pENTR1A-FLAG-HA-H2ABbd construct. The CSIV-TRE-RfA-UbC-KT FLAG-HA-H2ABbd vector was generated as described above.

Lentiviral Transduction—Lentivirus expressing the respective genes was generated by the co-transfection of 293T cells with pCMV-VSV-G-RSV-RevB (a gift from H. Miyoshi), pCAG-HIVgp (also a gift from H. Miyoshi), and the respective CSIV-TRE-RfA-UbC-KT using the calcium phosphate co-precipitation method. Cells infected with viruses were treated with 2 μg/ml puromycin (Sigma-Aldrich) for 2 days. To express the inducible gene, doxycycline (Dox; Sigma-Aldrich) was added to the medium at a concentration of 1 μg/ml.

Immunoblotting—Collected cells were washed with ice-cold PBS, and sample buffer was added to cell pellets. Samples were boiled for 5 min and used as total cell lysate. Chromatin fractionation was performed as described previously (16). Antibodies used in this study are listed in Table 1.

Cell Cycle Synchronization—HeLa EGFP-H2A and H2ABbd cells were first synchronized at the G_1/S boundary by exposure to 2 mM thymidine for 18 h and then released into S phase by washout of thymidine with PBS and the addition of medium. After 8 h at release, these cells were exposed to 2 mM thymidine for 18 h and released again.

Cell Cycle Analysis—Cells were harvested and fixed with 70% ethanol. These were then washed once with PBS, treated with RNase, and stained with propidium iodide. Flow cytometry

TABLE 1
Antibodies used in this study

Antibody	Product number	Company
GFP	11814460001	Roche Applied Science
H2ABbd	06-1319	Millipore
H2A	ab18255	Abcam
H2AX	ab11175	Abcam
H3	ab1791	Abcam
PP2A	05-421	Upstate Biotechnology
γ-H2AX	JBW301	Millipore
Caspase3	9662	Cell Signaling
Cleaved Caspase3	9661	Cell Signaling
actin	ab6276	Abcam
ATM pS1981	AF1665	R&D Systems
ATM	sc23921	Santa Cruz Biotechnology
53BP1pS1778	2675	Cell Signaling
53BP1	sc22760	Santa Cruz Biotechnology
Chk2 pT68	2661	Cell Signaling
Chk2	sc9064	Santa Cruz Biotechnology
RPA2	2208	Cell Signaling
Cleaved caspase 6	9761	Cell Signaling
IκB-α	sc203	Santa Cruz Biotechnology
p65	sc372	Santa Cruz Biotechnology
SP1	sc14027	Santa Cruz Biotechnology

TABLE 2
Primers used in this study

Sample	Sequence
H2A-F	AAAGAATTCAATGTCTGGTCGTGGCAAGCAAG
H2A-R	AAAGATATCTCACTTGCCCTTTGCCTTGTG
H2AX-F	AAAGAATTCAATGTCGGGCCGCGGCAAGAC
H2AX-R	AAAGATATCTTAGTACTCCTGGGAGGCCTG
H2ABbd-F (EcoRI)	AAAAGCTTAATGCCGAGGAGGAGGAGACG
H2ABbd-R (NotI)	AAAGCGGCCGCCTAGTCCTCGCCAGGGGCC
H2ABbd-F (XhoI)	AAACTCGAGATGCCGAGGAGGAGGAGACG
FLAG-HA-H2ABbd-F	AAAGAATTCGCCACCATGGACTACAAGGACGACG
GAPDH-F	GCCAATCTCAGTCCCTTCC
GAPDH-R	TAGTAGCCGGGCCCTACTTT
IκB-α-F	CAGCAGCTCACCGAGGA
IκB-α-R	GGCCAGGTCTCCCTTCA
BIK-F	TCTGCCTGCTGCACTTTG
BIK-R	TCTGCCTGCTGCACTTTG
NKX3.1-F	TGTGACCCTTGCACCAAA
NKX3.1-R	GACAAAGCCACCCCAAGTT
p21-F	TCTGCCTGCTGCACTTTG
p21-R	TCTGCCTGCTGCACTTTG

was performed using a FACS CANTO2 flow cytometer (BD Biosciences).

DNA Fragmentation Assay—Cells were lysed in 10 mM Tris-HCl (pH 8.0) buffer containing 0.6% SDS and 10 mM EDTA and incubated with 100 μg/ml RNase. After 1 h, NaCl was added to a final concentration of 1 M and incubated for 1 h at 4 °C. Lysates were centrifuged (12,500 rpm, 20 min, 4 °C). The supernatants were extracted with phenol/chloroform. DNA was precipitated for 30 min in 3 volumes of ethanol at −80 °C and centrifuged (17,900 × *g*, 10 min, 4 °C). The pellet was dissolved in 100 μl of H_2O. DNA was resolved by electrophoresis at 100 V for 30 min on 1% agarose gels and stained with 0.1 μg/ml ethidium bromide.

Time Lapse Microscopy—Cells were cultured in 35-mm glass bottom culture dishes (Greiner Bio-one). Medium was changed to a phenol red-free one after doxycycline was added. The dishes were mounted on a fluorescence microscope (Zeiss LSM710) equipped with a video camera. The temperature of the medium was kept constant at 37 °C and CO_2 concentration at 5% using a heated stage. Time lapse images were captured every 20 min, and *z*-stacks of the images were obtained every 2 μm, using a PlanApochromat ×40/1.4 numerical aperture oil lens (Carl Zeiss) as objectives, and were processed by the ZEN 2013 software (Carl Zeiss).

Micrococcal Nuclease (MNase) Assay—Cells were collected after release from thymidine block and permeabilized with 0.01% L-α-lysophosphatidylcholine (Sigma) in 150 mM sucrose, 80 mM KCl, 35 mM HEPES (pH 7.4), 5 mM K_2HPO_4, 5 mM Mg2Cl, and 0.5 mM $CaCl_2$ for 90 s. Cells were washed and suspended with 20 mM sucrose, 50 mM Tris (pH 7.5), 50 mM NaCl, and 2 mM $CaCl_2$ (MNase buffer). The same amounts of MNase buffer containing MNase (2 units/ml) were added and incubated at room temperature for various times. DNA was isolated and subjected to 0.8% agarose gel electrophoresis.

Real-time PCR—Total RNA was isolated as described previously (17). 50 ng of RNA was reverse-transcribed with random primers using Thermoscript RT-PCR (Invitrogen). Quantitative real-time PCR was performed using Power SYBR Green (Applied Biosystems) and the real time PCR machine ABI7900HT (Applied Biosystems). Expression levels were normalized to GAPDH. Primers used in real-time PCR are listed in Table 2.

Microarray Experiment—RPE FLAG-HA H2ABbd cells were synchronized at G_0 phase with DMEM containing 0% FBS and collected, and total RNA was prepared using ISOGENII (Nippongene). RNA hybridization, wash, and analysis were performed using SurePrint G3 Human GE 8x60k version 2.0 (Agilent Technologies) and GeneSpring GX version 12.6.0 (Agilent Technologies). Microarray expression profiling was performed by Oncomics (Nagoya, Japan).

Microarray and Publicly Available RNA-seq, ChIP-seq Data Analysis—Up-regulated and down-regulated genes were identified by measuring Cy3 and Cy5 probe intensities. Genes that showed elevated or reduced expression (greater or less than 2-fold compared with the control) at the 8 and 16 h time points were listed, and the two groups (8 and 16 h) were compared with identify overlapping/common factors. The odds ratio was calculated as follows, (genes overlapping (common to both 8 and 16 h) × genes not included in either the 8 or 16 h group)/(genes unique for group 1 (8 h) × genes unique for group 2 (16 h)). Representation factor and *p* value for exact hypergeometric probability were calculated as described previously. RNA-seq data for different staged of male germ cell development was retrieved from the Gene Expression Omnibus (series accession number GSE35005). BedGraph files for control and H2ABbd siRNA knockdown and H2ABbd ChIP-seq experiments were obtained from the data (series accession number GSE38771) deposited by Tolstorukov *et al.* (11). FPKM values for control and H2ABbd siRNA knockdown experiments were generously provided by Tolstorukov *et al.*[5] University of Toronto BAR (Bio-Analytic Resource) tools were used for heat map analysis. Wig and BedGraph files were uploaded into the IGV Genome Browser (Broad Institute), and images were obtained for respective gene loci.

[5] M. Y. Tolstorukov, J. A. Goldman, C. Gilbert, V. Ogryzko, R. E. Kingston, and P. J. Park, personal communication.

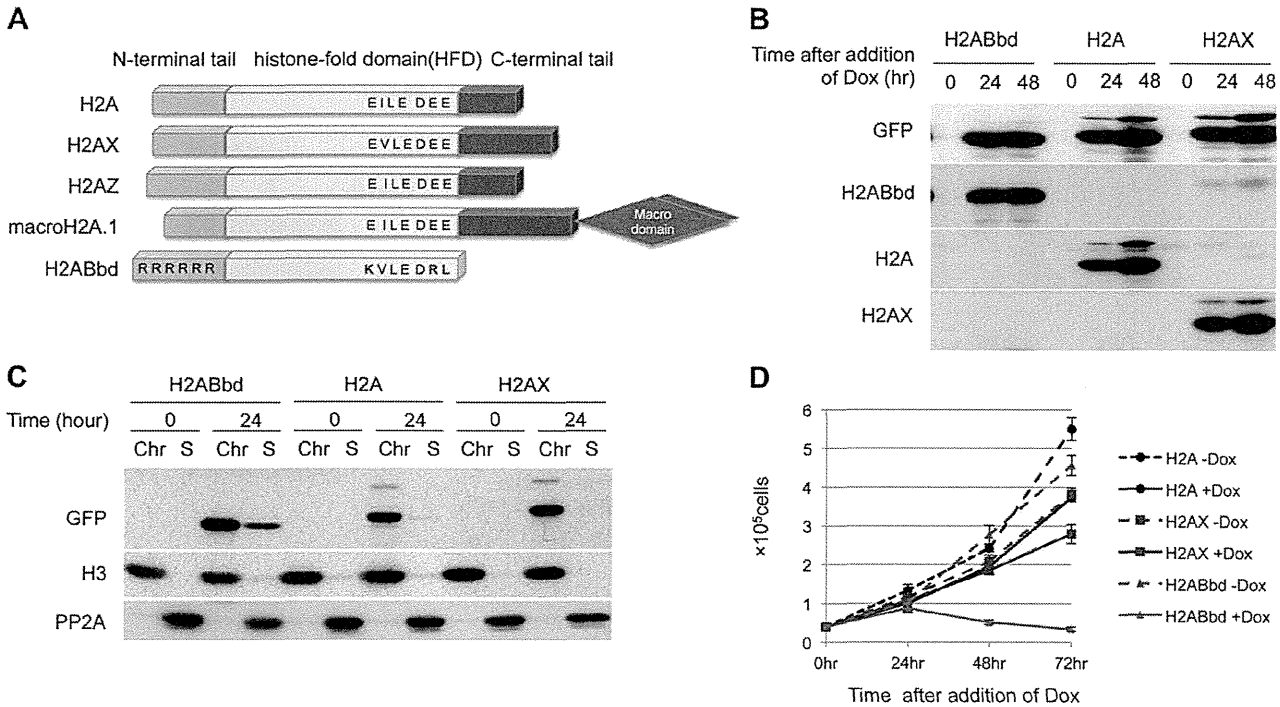

FIGURE 1. **Induction of H2ABbd inhibits proliferation of HeLa cells.** *A*, schematic representation of the histone H2A variants. The C-terminal domain is not conserved among the H2A variants. In particular, H2ABbd does not contain both the acidic patch and the C-terminal region. *B*, immunoblot analyses showing the time course of EGFP-tagged H2ABbd, H2A, or H2AX induction. HeLa cells transfected with Dox-inducible EGFP-tagged H2ABbd, H2A, or H2AX were cultured in the presence of Dox for the indicated amount of time. Cells were collected, and total cell extracts were subjected to immunoblotting using the respective antibodies indicated in the figure. *C*, cells were collected as in *B*, followed by chromatin fractionation and immunoblot analysis. Each type of histone was detected in the chromatin fraction. *D*, 50,000 HeLa cells were seeded and cultured in the presence of Dox to express EGFP-tagged H2ABbd, H2A, or H2AX. At the indicated time points after the addition of Dox, cell numbers were counted. Data are presented from three independent experiments. *Error bars*, S.D.

RESULTS

Overexpression of H2ABbd, but Not H2A and H2AX, Results in Growth Defect—The most recently discovered H2A variant, H2ABbd, possesses an acidic patch smaller than that of canonical H2A and lacks the C-terminal domain for interaction with H3 within the nucleosome (3) (Fig. 1*A*). To understand the physiological functions of this histone variant, we established cell lines expressing N-terminal EGFP-tagged H2ABbd, H2A, or H2AX that could be induced by Dox. EGFP-H2ABbd, -H2A, or -H2AX was clearly detectable at 24 h after the addition of Dox in nearly all cells, although the expression level was varied (supplemental Fig. 1*A*).

EGFP-tagged H2A or its variants were expressed in almost same level 24 and 48 h after the addition of Dox (Fig. 1*B*). In this system, the level of ectopically expressed EGFP-H2A was slightly stronger than in endogenous H2A, whereas the EGFP-H2AX level was far higher than in endogenous H2AX. Because H2ABbd is expressed robustly in postmeiotic germ cells (18), endogenous H2ABbd was hardly detectable in HeLa cells. Importantly, subcellular fractionation revealed that ectopically expressed EGFP-H2A and its variants were incorporated into the chromatin fraction in similar levels (Fig. 1*C*).

HeLa cells expressing EGFP-H2ABbd exhibited marked reduction in the proliferation rate in the presence of Dox (Fig. 1*D*), showing an increase in the populations of S phase cells at 24 h and sub-G_1 at 48 h (supplemental Fig. 1*B*). In contrast, the effects of EGFP-H2A or EGFP-H2AX expression on cell growth were negligible. Taken together, these results indicate that expression of EGFP-H2ABbd specifically inhibits cell proliferation.

Overexpression of H2ABbd Triggers Caspase 3-dependent Apoptosis—As shown in Fig. 2*A*, 48 h after induction of EGFP-H2ABbd, most cells became round and detached from culture dishes. These cells were identified as non-mitotic cells by FACS analysis (supplemental Fig. 1*B*), suggesting that EGFP-H2ABbd expression induced apoptosis. In order to confirm whether the effect of H2ABbd is cell type-specific, we expressed FLAG-HA-tagged H2ABbd in MEFs and RPE cells (Fig. 2*A*). Similar to HeLa, FLAG-HA-H2ABbd strongly suppressed proliferations of MEFs and RPE cells through induction of cell death. The DNA fragmentation assay revealed that short DNA strands were readily detectable in HeLa and RPE cells expressing EGFP-H2ABbd or FLAG-HA-H2ABbd (Fig. 2*B*), confirming induction of apoptosis. Further, live cell imaging detected numerous apoptotic cells within 30 h after the induction of EGFP-H2ABbd prior to nuclear envelope breakdown and chromosome separation (Fig. 2*C*). These results suggest that apoptosis induced by the expression of EGFP-H2ABbd was not caused by mitotic catastrophe. Consistent with this observation, we detected the cleaved form of caspase 3 in EGFP-H2ABbd- or FLAG-HA-H2ABbd-expressing HeLa and RPE cells with a concomitant decrease in the level of procaspase 3 (Fig. 2*D*). Importantly, low and moderate expression of EGFP-H2ABbd did not

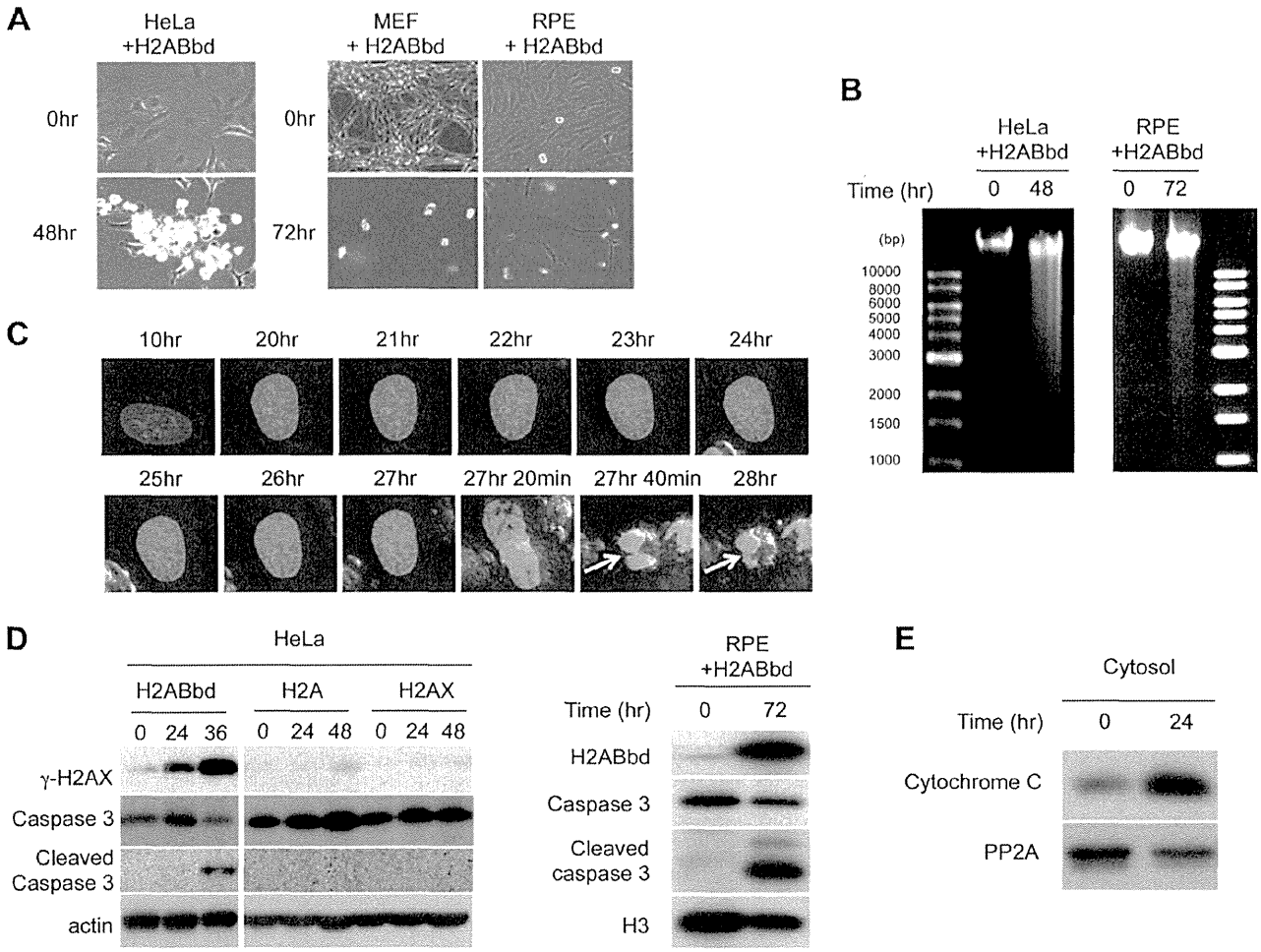

FIGURE 2. **Analysis of H2ABbd-induced apoptosis in HeLa cells.** *A*, EGFP-tagged H2ABbd was induced for 48 or 72 h in HeLa or MEF, respectively. FLAG-HA-H2ABbd was induced for 72 h in RPE cells. Typical differential interference contrast images are shown. *B*, DNA fragmentation was observed in HeLa cells expressing EGFP-H2ABbd for 48 h or in RPE cells expressing FLAG-HA-H2ABbd for 72 h. Cells were prepared as described in *A* and lysed, and DNA fragments were analyzed by agarose gel electrophoresis. *C*, EGFP-H2ABbd was expressed after the addition of Dox in HeLa cells and subjected to time lapse microscopy. Images were captured at the indicated time points. *Arrows* (27 h 40 min and 28 h time points) show cells starting to undergo apoptosis. *D*, immunoblot analyses showing the time course of EGFP-tagged H2ABbd, H2A, or H2AX induction. Cells were collected at the indicated times after induction, and total cell extracts were subjected to immunoblotting using the respective antibodies. *E*, cytosol fraction was prepared from HeLa cells with/without Dox for 24 h and subjected to immunoblot analysis to detect cytochrome *c*.

trigger apoptosis and activation of procaspase 3. Therefore, the induction of apoptosis appeared dose-dependent (supplemental Fig. 2, *A–C*) and thus might explain the survival of cells expressing H2ABbd reported previously. In addition, untagged H2ABbd also induced apoptosis as effectively as EGFP-H2ABbd did, eliminating the possibility that apoptosis was not due to an indirect consequence of EGFP tagging into the H2ABbd molecule.

We next asked whether H2ABbd overexpression caused cytoplasmic release of cytochrome *c*, which binds with Apaf1 to activate a series of caspase cascades (19). After induction of H2ABbd, cytochrome *c* was readily detected in the cytoplasmic fraction (Fig. 2*E*). In summary, our results indicate that overexpression of EGFP-H2ABbd triggers caspase-dependent apoptosis mediated by cytochrome *c* release.

Ectopic Expression of H2ABbd Causes DNA Damage—Incorporation of H2ABbd into nucleosomes could result in destabilization of nucleosomes, generating nucleosome-poor regions that easily cause spontaneous DNA damage. In order to investigate whether incorporation of H2ABbd into chromatin actually caused nucleosome-poor regions and whether apoptotic cell death was caused by the activation of DNA damage checkpoints, we synchronized cells at G_1/S by double thymidine block and induced expression of EGFP-H2ABbd or -H2A, as shown in Fig. 3*A*. MNase treatment of cells expressing H2ABbd or H2A revealed that that from cells expressing H2ABbd was far more sensitive than chromatin from cells expressing H2A even at early S phase (Fig. 3*B*). In addition, the nucleosomal ladder became degraded in H2ABbd-expressing cells but not in H2A-expressing cells, showing increased signal between the nucleosomal bands. These destabilizations were also observed in cells expressing H2ABbd even at early S phase (Fig. 3*C*). Taken together, these results strongly suggested that incorporation of H2ABbd into chromatin probably resulted in destabilizing nucleosomes. FACS analysis revealed that cells expressing EGFP-H2A normally progressed through S phase and com-

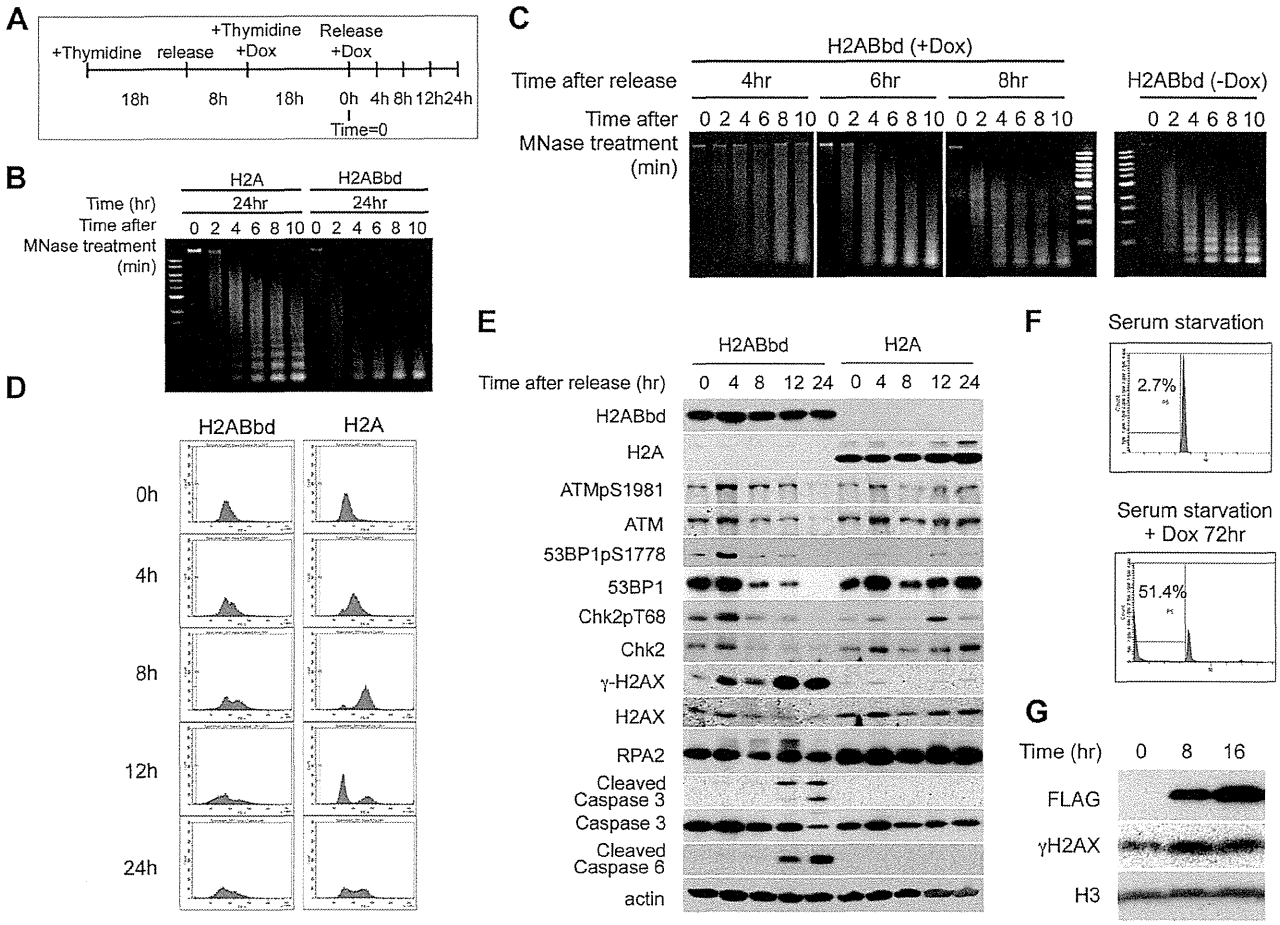

FIGURE 3. **Overexpression of H2ABbd induces DNA damage during S phase.** *A*, the experimental strategy to synchronize HeLa cells in G_1/S phase by double thymidine block and induce H2ABbd or H2A expression after the addition of Dox is shown. Cells were released from the thymidine block at 0 h, and samples were taken. *B*, cells expressing EGFP-H2ABbd and EGFP-H2A were collected at 24 h after release and subjected to MNase analysis. DNA was isolated from cells after MNase treatment for the indicated time (min) and subjected to agarose gel electrophoresis. *C*, EGFP-H2ABbd-expressing cells were collected at the indicated times after release and subjected to MNase analysis (*left*). As a control, the data from HeLa cells without induction of H2ABbd are also shown (*right*). *D*, cells prepared as in *A* were collected at the indicated times after thymidine block for FACS analysis. *E*, total cell extracts were subjected to immunoblotting using the indicated antibodies. *F*, RPE cells were cultured in medium without FBS for 5 days to synchronize in G_0 (*left*) or further incubated in the serum-starved condition with Dox for 72 h (*right*) to express FLAG-HA-tagged H2ABbd. *G*, RPE cells were cultured in medium without FBS for 5 days and further incubated in the presence of Dox. At 8 or 16 h after the addition of Dox, cells were collected, and total cell extracts were subjected to immunoblotting using antibodies as indicated in the figure.

pleted DNA replication within 8 h (Fig. 3*D*). In contrast, cells expressing EGFP-H2ABbd showed a severe defect in S phase progression and a marked increase in sub-G_1 population prior to the completion of S phase. As demonstrated in Fig. 3*E*, a strong signal of γ-H2AX was detected in HeLa cells expressing H2ABbd 4 h after release. Given that apoptosis was induced 12 h after release, as judged by cleaved caspase 3, this γ-H2AX signal was probably due to DNA damage but not DNA fragmentation as a consequence of apoptosis. Indeed, two-color flow cytometric analysis using propidium iodide and antibodies to γ-H2AX revealed that γ-H2AX-positive cells were detected in S phase, but not sub-G_1 phase cells (supplemental Fig. 3). Further, association of DNA damage in cells expressing EGFP-H2ABbd with DNA replication suggested the activation of the intra-S phase checkpoint. Therefore, we examined the activation of target proteins of DNA damage checkpoint kinases. As exhibited in Fig. 3*E*, hyperphosphorylated RPA2 and phosphorylation of ATM at Ser-1981 (a marker of ATM activation) were significantly up-regulated in cells expressing EGFP-H2ABbd. ATM activation was also confirmed by phosphorylations of 53BP1 and Chk2. DNA replication-induced DNA damage and activation of intra-S phase checkpoint were not detected in cells expressing EGFP-H2A. We went on to examine whether apoptosis induced by the expression of H2ABbd was caused by aberrant DNA replication. RPE cells expressing FLAG-HA-H2ABbd were synchronized at quiescent state by serum starvation. Surprisingly, ectopic expression of EGFP-H2ABbd induced cell death in the quiescent cells, showing that H2ABbd-mediated apoptosis could occur without DNA replication (Fig. 3*F*). In particular, accumulation of γ-H2AX was also observed (Fig. 3*G*), further confirming that H2ABbd is associated with DNA damage. Collectively, these observations suggest that H2ABbd overexpression-mediated cell death is not restricted to DNA damage during S phase.

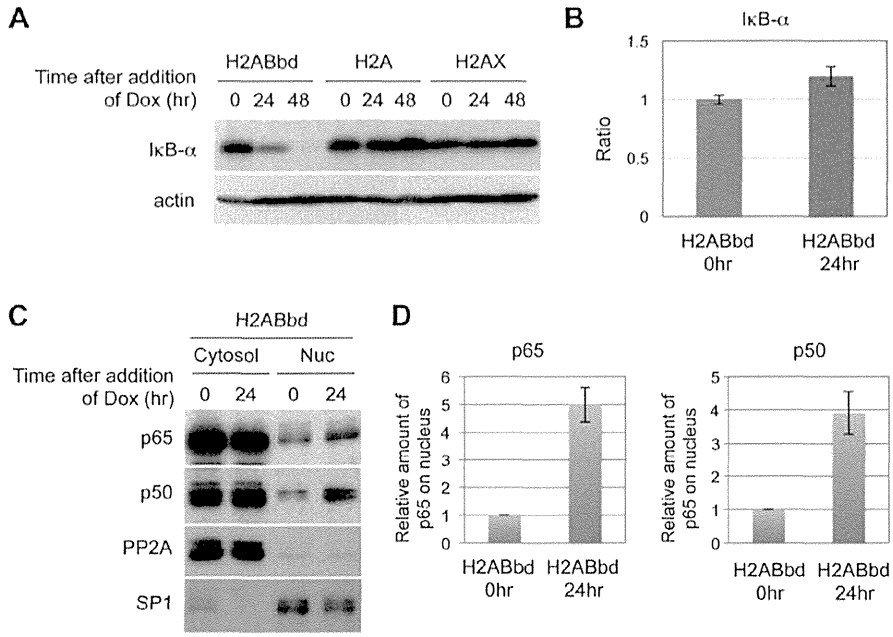

FIGURE 4. **NF-κB signaling cascade was activated upon overexpression of H2ABbd.** *A*, degradation of inhibitor of NF-κB, IκB-α, was observed in HeLa cells overexpressing EGFP-H2ABbd. *B*, IκB-α mRNA was not decreased upon H2ABbd expression. Total RNAs were prepared from asynchronous HeLa cells (72 h after the addition of Dox). Quantitative real-time RT-PCR was performed using a set of primers for the IκB-α transcript. Relative mRNA expression was normalized to GAPDH. *C*, NF-κB activation was observed in H2ABbd-expressing HeLa cells. Cells were treated with Dox for 24 h to induce EGFP-H2ABbd or EGFP-H2A, collected for subcellular fractionation, and subjected to immunoblotting. PP2A and SP1 were used as markers of the cytosol fraction and nuclear fraction, respectively. *D*, p65 and p50 were accumulated in nucleus upon the addition of Dox. The signal intensity was analyzed by ImageJ software and normalized with SP1. Data are presented from three independent experiments. *Error bars*, S.D.

NF-κB Is Activated by H2ABbd Expression—Given that NF-κB plays a role in the induction of apoptosis, we examined whether activation of NF-κB occurred in cells expressing EGFP-H2ABbd. Indeed, we found that IκB-α was markedly decreased in cells expressing EGFP-H2ABbd (Fig. 4*A*). Reduced IκB was presumably caused by enhanced degradation because the amount of IκB-α transcript did not change despite the reduction in the protein level (Fig. 4*B*). Consistent with this, we found that a fraction of p65 and p50 proteins translocated into the nucleus when EGFP-H2ABbd was expressed (Fig. 4, *C* and *D*). Small fractions of p50 and p65 already existed in non-treated cells; however, this level was increased upon H2ABbd induction. In short, these results indicate that H2ABbd expression activated the NF-κB signaling pathway.

Apoptosis Induced by the Expression of H2ABbd Is Dependent on the Activation of Caspase 3 and NF-κB—We examined whether apoptosis induced by H2ABbd was dependent on caspase 3 activation. Treatment with pan-caspase inhibitor benzyloxycarbonyl-VAD-fluoromethyl ketone (*Z-VAD*) for 48 h inhibited EGFP-H2ABbd-induced activation of caspase 3 (Fig. 5*A*) and suppressed apoptosis, as well as showing significant reduction in the sub-G_1 population (25.3% *versus* 9.2%) (Fig. 5*B*). Intriguingly, treatment with inhibitors of NF-κB, aminosalicylic acid (ASA) (20) and ammonium pyrrolidine dithiocarbamate (21), markedly suppressed degradation of IκB-α, and the activation of caspase 3 (Fig. 5*C* and supplemental Fig. 4*A*). Suppression of EGFP-H2ABbd-dependent apoptosis was further confirmed by the observation that ASA or ammonium pyrrolidine dithiocarbamate treatment reduced sub-G_1 fraction cells (25.3% *versus* 12.4%, 22.4% *versus* 3.6%) (Fig. 5*B* and supplemental Fig. 4*B*). As a control, we treated HeLa cells to induce apoptosis under NF-κB inhibitors. Consistent with previous reports, inhibition of NF-κB could suppress UV-induced apoptosis (Fig. 5, *B* and *D*) and UV-, 4NQO-, and actinomycin D-induced apoptosis (supplemental Fig. 4, *C* and *D*).

Expression of H2ABbd Perturbs Gene Transcription Profiles—To gain further insight into the changes in the transcriptional network upon ectopic expression of H2ABbd in RPE cells, we performed gene expression microarray analysis in control (0 h) and H2ABbd-induced (8 and 16 h) cells. In order to avoid indirect effects of H2ABbd expression, we chose relatively early time points after H2ABbd expression. 1714 and 3733 genes were found to be up-regulated (>2-fold) after 8 and 16 h, respectively (Fig. 6*A*; full list given in supplemental Table 1). Comparison of the 8 and 16 h gene sets showed significant overlap, with 1024 genes in common. Further, statistical analyses revealed that the odds ratio and representation factor for overlap were 8.5 (>2 is generally significant) and 3.2 (>1 is generally significant), respectively (Fig. 6*A*). The *p* value for association was nearly equal to zero, suggesting that the overlap between the 8 and 16 h groups was not random. Previous studies have investigated the roles of H2ABbd in human cells by gene knockdown experiments (10). Interestingly, some of the genes, such as *ARC*, *BLK*, and *ICAM5*, that are repressed upon H2ABbd knockdown exhibited transcriptional up-regulation upon enforced H2ABbd expression in our study (supplemental Fig. 6*A*). These results further supported our hypothesis that there is a functional link between H2ABbd and regulation of gene transcription.

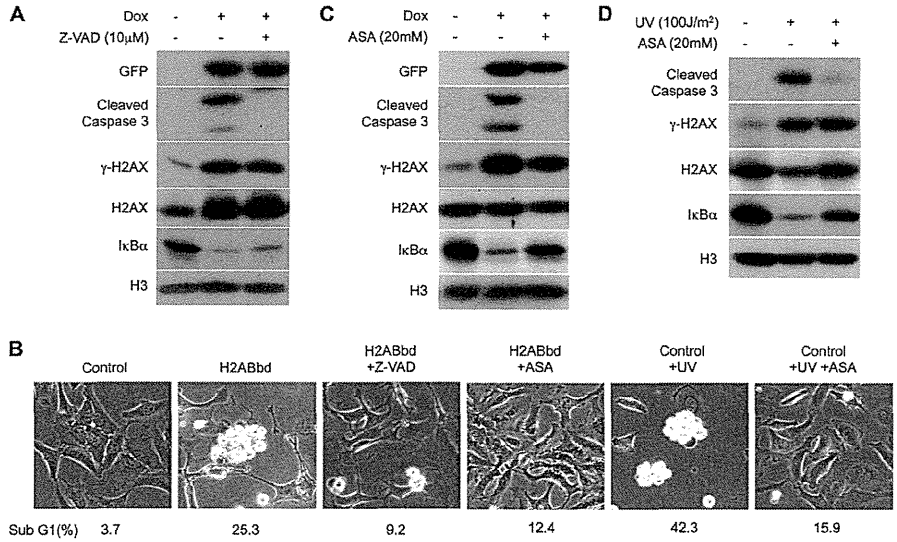

FIGURE 5. **H2ABbd-mediated apoptosis was blocked by caspase inhibitor and NF-κB inhibitor.** *A*, HeLa cells were treated with or without Dox and benzyloxycarbonyl-VAD-fluoromethyl ketone (*Z-VAD*) (10 μM), a pancaspase inhibitor, for 48 h. Total cell extracts were prepared for immunoblotting. *B*, HeLa cells were treated with or without Dox, benzyloxycarbonyl-VAD-fluoromethyl ketone (10 μM), or ASA (20 mM), an inhibitor of NF-κB, for 48 h. As a control, HeLa cells were irradiated with UV (100 J/m^2) and cultured with or without ASA (20 mM) for 48 h. Typical differential interference-contrast images and sub-G_1 DNA contents (percentages) analyzed by FACS are shown. *C*, HeLa cells were treated with or without Dox and ASA (20 mM) for 48 h. Total cell extracts were prepared for immunoblotting. *D*, HeLa cells were irradiated with UV (100 J/m^2) and cultured with or without ASA for 48 h, and total cell extracts were prepared and analyzed by immunoblotting.

As for the down-regulated loci, we found that the expression of 1300 and 2891 genes was reduced by more than 2-fold after 8 and 16 h of H2ABbd induction, respectively. This association was also highly significant, with 1084 genes in common. The odds ratio for overlap was ~47, the representation factor was 5.8, and the *p* value was nearly zero (Fig. 6*A*).

Up-regulated Genes upon H2ABbd Expression Exhibit Association with Reproductive Functions—To categorize up-regulated and down-regulated genes in H2ABbd-overexpressing cells, we carried out GO tests. GO analysis revealed that development- and differentiation-associated genes were predominantly enriched among common up-regulated genes (Fig. 6*B*). It is interesting to note that H2ABbd is expressed in differentiated germ cells, such as elongating and round spermatids (Fig. 7*A*). Thus, selective activation of differentiation-associated genes might reflect the biological function of H2ABbd to regulate such genes during germ cell development. To examine this point further, we carried out functional clustering of the up-regulated genes by using the publicly available DAVID (Database for Annotation, Visualization, and Integrated Discovery) Functional Classification Tool. Indeed, this analysis revealed that the up-regulated genes were enriched in a functional cluster (cluster 14) enriched for germ cell- and reproductive function-associated GO terms, such as male genitalia development (GO:0030539) and spermatogenesis (GO:0007283). The association between the genes and functional terms in this group is shown in a two-dimensional view heat map (supplemental Fig. 7*A*). A positive gene term association that passes the statistical filter assigned by DAVID is given a value of 1 (shown in *red*), and an association that has not been reported yet is denoted with 0 (shown in *black*). The enrichment score of for this functional category was 2.1, which is statistically significant (in general, scores of >1 are accepted as significant).

Previous studies have reported that H2ABbd is expressed robustly in postmeiotic germ cells. To further examine this point, we retrieved comprehensive RNA sequencing (RNA-seq) data for different stages of murine male germ cell development from the publicly available Gene Expression Omnibus database (18). Transcription of *H2afb1*, the murine homolog of human *H2ABbd*, could be detected only in the postmeiotic elongating and round spermatids, but not in spermatogonia (Type A and B) or spermatocytes (leptotene, pachytene stages) (Fig. 7*B*). We asked whether the factors up-regulated by enforced H2ABbd expression in RPE cells included genes that are normally transcribed in postmeiotic germ cells. To this end, we checked the wig files provided in this data set by eye and selected ~100 genes that were up-regulated upon H2ABbd overexpression as well as demonstrating robust expression patterns in spermatid but not in progenitor cells, such as *DHRS2* (dehydrogenase/reductase member 2), *PDZK1IP1* (PDZK1-interacting protein 1), *PAQR9* (progestin and adipoQ receptor family member IX), and *AQP3* (aquaporin 3). These genes were classified as putative "spermatid-enriched genes" (Fig. 7, *A* and *B*, and supplemental Table 3).

In contrast, GOs enriched for common down-regulated genes (1084 annotations) were associated with cellular processes, such as cation binding, metal ion binding, and DNA binding. The full list of GOs is given in supplemental Table 2.

Overexpression of H2ABbd Activates Apoptosis-related Genes—Given the fact that overexpression of H2ABbd induces apoptosis, we wondered whether cell death-related genes were up-regulated after 8 and 16 h. Indeed, around 80 genes were found to be included in this category (representative genes shown by heat map in Fig. 6*C*; full list given in supplemental Fig. 5). Interestingly, well known proapoptotic factors, such as *BIK* (Bcl-2-interacting killer) and *BCL2L10* and *BCL2L11* (Bcl2-like pro-

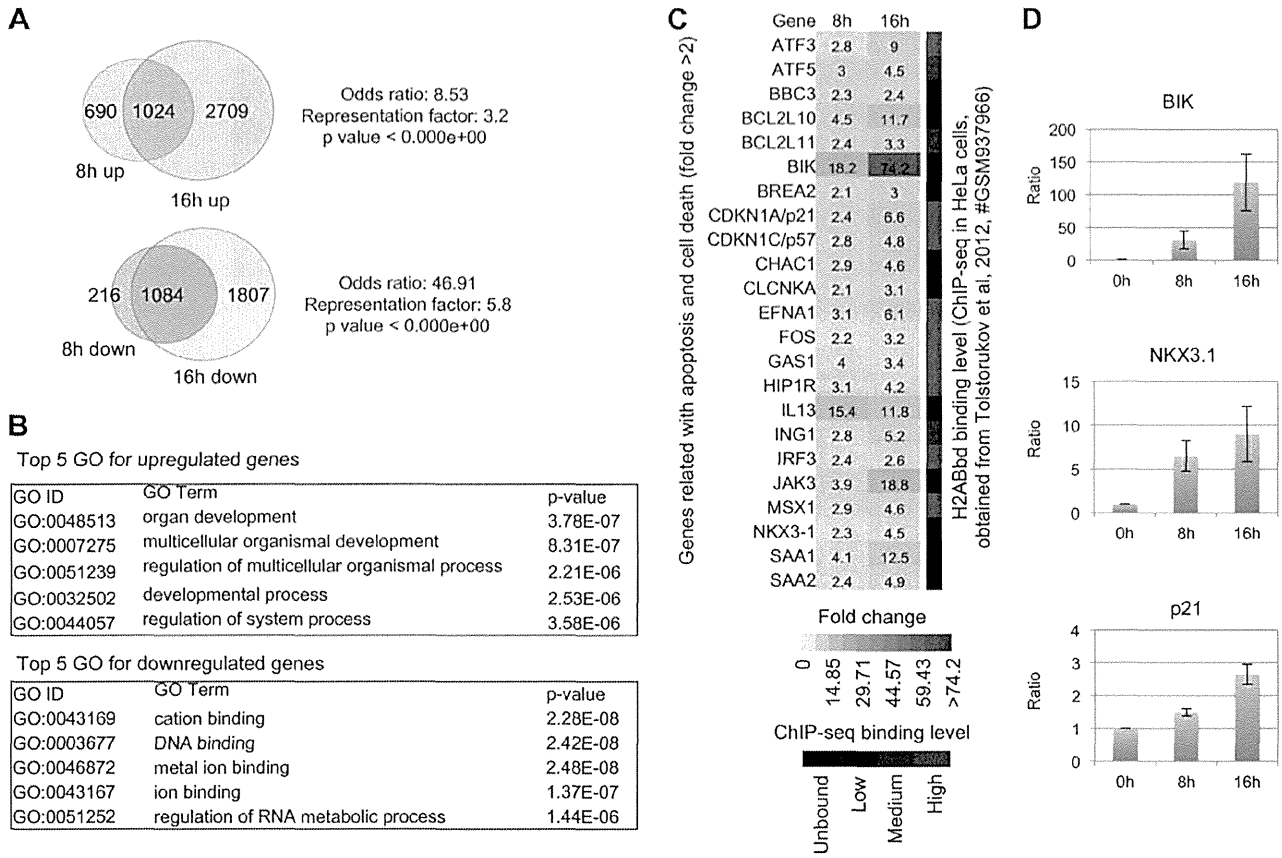

FIGURE 6. **Genes up-regulated and down-regulated upon enforced H2ABbd expression.** *A*, up-regulated and down-regulated genes upon enforced H2ABbd expression are summarized in Venn diagrams. 1024 genes were found to be activated (>2-fold) at both the 8 and 16 h time points after H2ABbd expression. In contrast, 1084 genes were repressed (<2 fold) after 8 and 16 h of enforced H2ABbd expression. The odds ratio, representation factor, and *p* value are shown *beside* the diagrams. *B*, top five GO categories for up-regulated and down-regulated genes, selected by statistical significances determined with *p* value, are shown within their respective *boxes*. *C*, a group of apoptosis- and cell death-related genes were up-regulated in H2ABbd-overexpressing cells. -Fold changes in gene expression (>2-fold) are demonstrated in a heat map (*left*). The *color scale* for the heat map is given *below*. The ratio of up-regulation (-fold change) for each gene is shown within its respective *box* inside the heat map. *Right*, summary of the H2ABbd deposition pattern obtained from previously published ChIP-seq data in HeLa cells for each gene. The level of enrichment was judged by eye from the BedGraph data visualized by IGV and for simplification categorized into four groups: unbound, low, medium, and high, respectively (demonstrated in a *black to red color scale* at the *bottom*). *D*, quantitative real-time PCR results for three randomly picked loci, namely *BIK*, *NKX3-1*, and *p21*, from the up-regulated gene list. The relative ratio of activation for these genes, compared with the control (0 h, value = 1), is demonstrated in *bar plots*. *Error bars*, S.D. ($n = 3$). The relative mRNA expression was normalized to GAPDH.

tein 10 and 11), were activated at the 8 and 16 h time points (Fig. 6*C*). We performed quantitative real-time PCR analysis for three randomly picked genes, *BIK*, *NKX3-1*, and *p21*, and found that these were up-regulated by nearly 100-, 10-, and 3-fold in 16 h samples (Fig. 6*D*, results shown for 8 and 16 h). These results were highly similar to our microarray data, suggesting the reproducibility of the findings. In addition, functional tests using DAVID tools demonstrated that up-regulated genes could be clustered in an apoptosis-related group (functional cluster 43), showing association with terms such as regulation of caspase activity (GO:0006919) and apoptosis regulator Bcl2, BH (IPR000712) (supplemental Fig. 7*B*). The enrichment factor for this cluster was >1 (1.09).

The ChIP-seq deposition pattern of H2ABbd in human (HeLa) cells has been already reported (10). We wondered whether apoptosis-related genes, identified from our study, demonstrated H2ABbd enrichment in HeLa cells. Indeed, we found that many of these loci, such as CDKN1A, MSX1, and ATF3, showed H2ABbd deposition around the promoter and/or gene body regions. The level of H2ABbd enrichment (strong, moderate, and low) for apoptosis-associated factors is shown at the *right side* of the gene expression heat map (Fig. 6*C* and supplemental Fig. 6*B*). Collectively, these results suggest that at least some of the apoptosis-related loci could be marked by a basal level of H2ABbd enrichment in wild type cells. Upon increased H2ABbd binding due to some cellular cues/signals, these genes could be switched on in turn and contribute to the observed apoptotic phenotype in our study.

DISCUSSION

Previous studies examining the role of the murine homolog of H2ABbd have suggested that this histone variant plays a role in spermatogenesis via promoting apoptosis of male germ cells. However, the mechanisms underlying H2ABbd-mediated apoptosis are not fully understood. In the present study, we found that ectopic expression of human H2ABbd specifically induced NF-κB-dependent apoptosis in a dose-dependent manner,

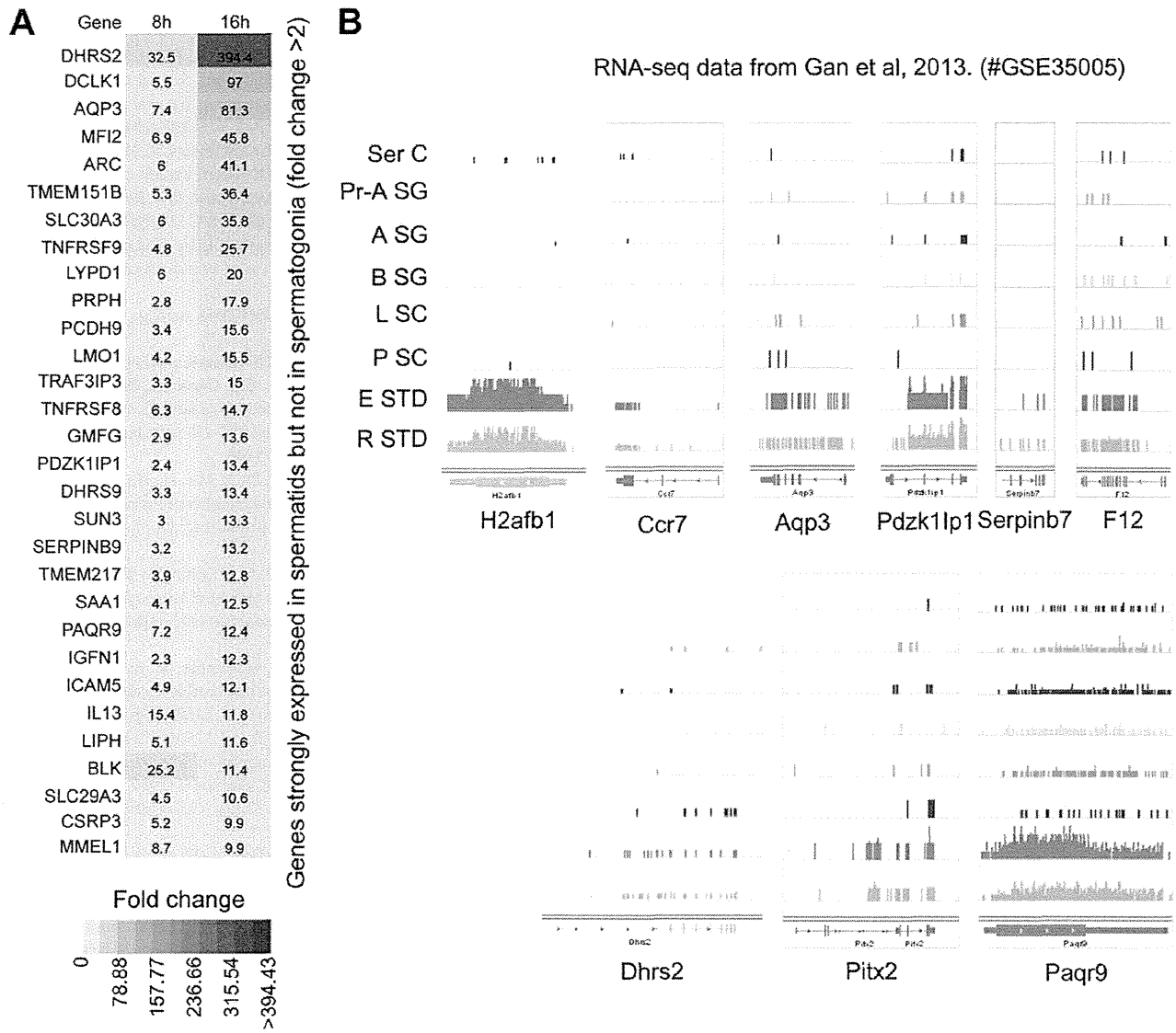

FIGURE 7. **An *in vivo* link between postmeiotic germ cell-specific gene expression and H2ABbd.** *A*, genes up-regulated upon H2ABbd expression in RPE cells included factors that are enriched in postmeiotic germ cells (*e.g.* in elongating and round spermatids). -Fold enrichment of such genes after 8 and 16 h are shown in a heat map. Similar to Fig. 6*C*, the ratio of up-regulation (>2-fold) is shown within the respective *boxes* for each gene, and the *color scale* is given *below*. *B*, comprehensive RNA-seq data for sertoli cells (*Ser C*, somatic cells in testis), primitive type-A spermatogonia (*Pr-A SG*), type-A spermatogonia (*A SG*), type-B spermatogonia (*B SG*), leptotene spermatocytes (*L SC*), pachytene spermatocytes (*P SC*), elongating spermatids (*E STD*), and round spermatids (*R STD*) were retrieved from the publicly available Gene Expression Omnibus database (18) (series accession number GSE35005). The expression of the murine H2ABbd homolog, H2afb1, is demonstrated on the *left*. The transcription levels for four other factors, namely *Dhrs2*, *Aqp3*, *Pdzk1Ip1*, and *Paqr9*, all of which are expressed specifically in the elongation and round spermatid cells, similar to *H2afb1*, are shown on the *right*.

showing that cell death during spermatogenesis may be in part dependent on NF-κB signaling.

Dysregulation of histone expression has been linked with increased mitotic chromosome loss and DNA damage sensitivity, resulting in genomic instability (22, 23), depending on the types or contexts of the histones (22). In this study, we noted that enforced expression of H2A or H2AX did not profoundly affect any cell function, although a slight delay of cell proliferation was observed (Fig. 1*D*). However, ectopic expression of H2ABbd led to drastic consequences, namely apoptosis.

Impairment of histone incorporation into chromatin leads to defects in chromatin assembly, causing stalled replication fork and leading to DNA replication-dependent DNA damage that activates ATM-dependent DDR pathways (24). Indeed, ectopic expression of H2ABbd caused DNA replication-dependent DNA damage, activating the intra-S phase checkpoint (Fig. 3, *C* and *D*). Surprisingly, ectopic expression of H2ABbd caused DNA damage even in quiescent cells (Fig. 3, *F* and *G*), suggesting that incorporation of H2ABbd into nucleosomes resulted in severe destabilization of nucleosomes and generation of anucleosome regions that might consist of fragile DNA sites.

Microarray analysis revealed that H2ABbd overexpression activates postmeiotic germ cell-enriched genes and apoptosis-related genes, although physiological implication of H2ABbd in

sperm cell differentiation or other developmental pathways remains elusive. This raises the possibility that H2ABbd could be selectively incorporated into specific gene loci to regulate transcription. However, any histone chaperone responsible for incorporation of H2ABbd into chromatin remains to be identified. We speculate that nucleosomal assembly of H2ABbd might be regulated by cooperation of histone chaperones and transcription factors that control development and differentiation of postmeiotic germ cells. Recently, it has been reported that human H2ABbd was deposited effectively at intron-exon boundaries in HeLa cells. Moreover, knockdown of H2ABbd resulted in splicing defect of mRNA, indicating that H2ABbd might be linked with regulation of splicing (11). Summarizing these possibilities, it could be speculated that expression of genes involved in development and/or postmeiotic germ cells could be mediated by the regulation of splicing of specific gene transcripts. In addition, recent genome-wide analysis showed that human H2ABbd was localized in both active and repressed chromatin domains (25). Thus, it should be important to determine the mechanism of how H2ABbd regulates the expression of genes involved in development and differentiation.

Acknowledgments—We thank Yoshie Chiba and Dr. Chisato Yamada for technical assistance and Dr. Mireille Delhase for critical reading of the manuscript. We also thank Drs. Peter J. Park and Michael Y. Tolstorukov (Massachusetts General Hospital, Boston, MA) for generously providing the RNA-seq FPKM data for control and H2Abbd knockdown experiments previously reported by Tolstorukov et al. (11).

REFERENCES

1. Lorch, Y., Zhang, M., and Kornberg, R. D. (1999) Histone octamer transfer by a chromatin-remodeling complex. *Cell* **96,** 389–392
2. Talbert, P. B., and Henikoff, S. (2010) Histone variants: ancient wrap artists of the epigenome. *Nat. Rev. Mol. Cell Biol.* **11,** 264–275
3. Chadwick, B. P., and Willard, H. F. (2001) A novel chromatin protein, distantly related to histone H2A, is largely excluded from the inactive X chromosome. *J. Cell Biol.* **152,** 375–384
4. Zhou, J., Fan, J. Y., Rangasamy, D., and Tremethick, D. J. (2007) The nucleosome surface regulates chromatin compaction and couples it with transcriptional repression. *Nat. Struct. Mol. Biol.* **14,** 1070–1076
5. Bao, Y., Konesky, K., Park, Y. J., Rosu, S., Dyer, P. N., Rangasamy, D., Tremethick, D. J., Laybourn, P. J., and Luger, K. (2004) Nucleosomes containing the histone variant H2A. Bbd organize only 118 base pairs of DNA. *EMBO J.* **23,** 3314–3324
6. Gautier, T., Abbott, D. W., Molla, A., Verdel, A., Ausio, J., and Dimitrov, S. (2004) Histone variant H2ABbd confers lower stability to the nucleosome. *EMBO Rep.* **5,** 715–720
7. Angelov, D., Verdel, A., An, W., Bondarenko, V., Hans, F., Doyen, C. M., Studitsky, V. M., Hamiche, A., Roeder, R. G., Bouvet, P., and Dimitrov, S. (2004) SWI/SNF remodeling and p300-dependent transcription of histone variant H2ABbd nucleosomal arrays. *EMBO J.* **23,** 3815–3824
8. Montel, F., Fontaine, E., St-Jean, P., Castelnovo, M., and Faivre-Moskalenko, C. (2007) Atomic force microscopy imaging of SWI/SNF action: mapping the nucleosome remodeling and sliding. *Biophys. J.* **93,** 566–578
9. Govin, J., Escoffier, E., Rousseaux, S., Kuhn, L., Ferro, M., Thévenon, J., Catena, R., Davidson, I., Garin, J., Khochbin, S., and Caron, C. (2007) Pericentric heterochromatin reprogramming by new histone variants during mouse spermiogenesis. *J. Cell Biol.* **176,** 283–294
10. Soboleva, T. A., Nekrasov, M., Pahwa, A., Williams, R., Huttley, G. A., and Tremethick, D. J. (2012) A unique H2A histone variant occupies the transcriptional start site of active genes. *Nat. Struct. Mol. Biol.* **19,** 25–30
11. Tolstorukov, M. Y., Goldman, J. A., Gilbert, C., Ogryzko, V., Kingston, R. E., and Park, P. J. (2012) Histone variant H2A. Bbd is associated with active transcription and mRNA processing in human cells. *Mol. Cell* **47,** 596–607
12. Shimada, M., and Nakanishi, M. (2006) DNA damage checkpoints and cancer. *J. Mol. Histol.* **37,** 253–260
13. Nowsheen, S., and Yang, E. S. (2012) The intersection between DNA damage response and cell death pathways. *Exp. Oncol.* **34,** 243–254
14. Wu, Z. H., Shi, Y., Tibbetts, R. S., and Miyamoto, S. (2006) Molecular linkage between the kinase ATM and NF-κB signaling in response to genotoxic stimuli. *Science* **311,** 1141–1146
15. Gu, C., Tong, Q., Zheng, L., Liang, Z., Pu, J., Mei, H., Hu, T., Du, Z., Tian, F., and Zeng, F. (2010) TSEG-1, a novel member of histone H2A variants, participates in spermatogenesis via promoting apoptosis of spermatogenic cells. *Genomics* **95,** 278–289
16. Shimada, M., Niida, H., Zineldeen, D. H., Tagami, H., Tanaka, M., Saito, H., and Nakanishi, M. (2008) Chk1 is a histone H3 threonine 11 kinase that regulates DNA damage-induced transcriptional repression. *Cell* **132,** 221–232
17. Shimada, M., Haruta, M., Niida, H., Sawamoto, K., and Nakanishi, M. (2010) Protein phosphatase 1gamma is responsible for dephosphorylation of histone H3 at Thr 11 after DNA damage. *EMBO Rep.* **11,** 883–889
18. Gan, H., Wen, L., Liao, S., Lin, X., Ma, T., Liu, J., Song, C. X., Wang, M., He, C., Han, C., and Tang, F. (2013) Dynamics of 5-hydroxymethylcytosine during mouse spermatogenesis. *Nat. Commun.* **4,** 1995
19. Danial, N. N., and Korsmeyer, S. J. (2004) Cell death: critical control points. *Cell* **116,** 205–219
20. Kopp, E., and Ghosh, S. (1994) Inhibition of NF-κB by sodium salicylate and aspirin. *Science* **265,** 956–959
21. Bessho, R., Matsubara, K., Kubota, M., Kuwakado, K., Hirota, H., Wakazono, Y., Lin, Y. W., Okuda, A., Kawai, M., and Nishikomori, R. (1994) Pyrrolidine dithiocarbamate, a potent inhibitor of nuclear factor κB (NF-κB) activation, prevents apoptosis in human promyelocytic leukemia HL-60 cells and thymocytes. *Biochem. Pharmacol.* **48,** 1883–1889
22. Meeks-Wagner, D., and Hartwell, L. H. (1986) Normal stoichiometry of histone dimer sets is necessary for high fidelity of mitotic chromosome transmission. *Cell* **44,** 43–52
23. Gunjan, A., and Verreault, A. (2003) A Rad53 kinase-dependent surveillance mechanism that regulates histone protein levels in *S. cerevisiae*. *Cell* **115,** 537–549
24. Ye, X., Franco, A. A., Santos, H., Nelson, D. M., Kaufman, P. D., and Adams, P. D. (2003) Defective S phase chromatin assembly causes DNA damage, activation of the S phase checkpoint, and S phase arrest. *Mol. Cell* **11,** 341–351
25. Ioudinkova, E. S., Barat, A., Pichugin, A., Markova, E., Sklyar, I., Pirozhkova, I., Robin, C., Lipinski, M., Ogryzko, V., Vassetzky, Y. S., and Razin, S. V. (2012) Distinct distribution of ectopically expressed histone variants H2A. Bbd and MacroH2A in open and closed chromatin domains. *PloS One* **7,** e47157

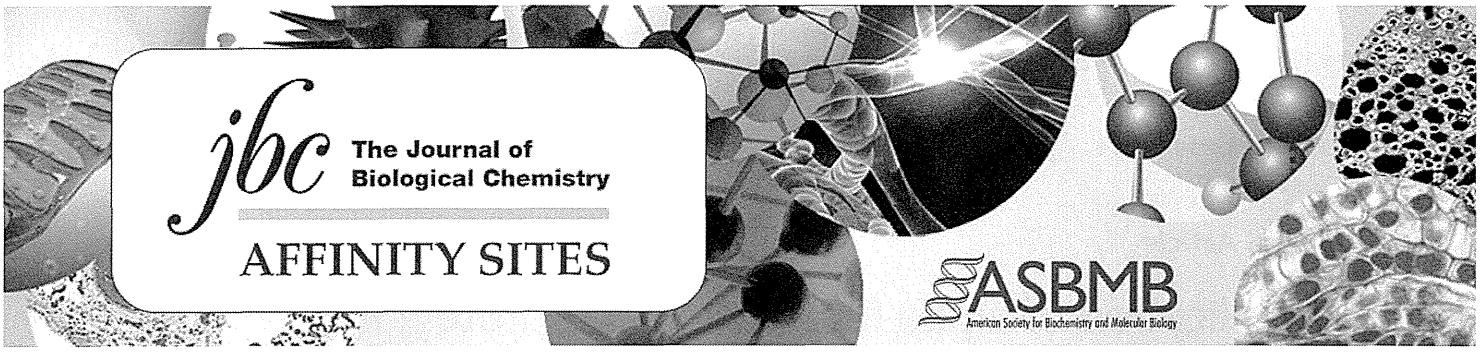

Cell Biology:

Mammal-specific H2A Variant, H2ABbd, Is Involved in Apoptotic Induction via Activation of NF-κB Signaling Pathway

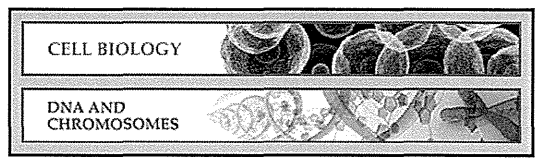

Takahiro Goshima, Midori Shimada, Jafar Sharif, Hiromi Matsuo, Toshinori Misaki, Yoshikazu Johmura, Kazuhiro Murata, Haruhiko Koseki and Makoto Nakanishi

J. Biol. Chem. 2014, 289:11656-11666.
doi: 10.1074/jbc.M113.541664 originally published online February 28, 2014
